

Zn isotope fractionation during uptake into marine phytoplankton: Implications for oceanic zinc isotopes

Journal Article**Author(s):**

Köbberich, Michael; Vance, Derek

Publication date:

2019-09-30

Permanent link:

<https://doi.org/10.3929/ethz-b-000366870>

Rights / license:

[Creative Commons Attribution-NonCommercial-NoDerivatives 4.0 International](#)

Originally published in:

Chemical Geology 523(S), <https://doi.org/10.1016/j.chemgeo.2019.04.004>

Funding acknowledgement:

143262 - The development and application of transition metal isotope systems in surface Earth geochemistry (SNF)

1 **Zn isotope fractionation during uptake into**
2 **marine phytoplankton: implications for**
3 **oceanic zinc isotopes**

4 **Michael Köbberich^{1*} and Derek Vance¹**

5 *To whom correspondence should be addressed

6 Submitted to: *Chemical Geology*

7 Special issue: *GEOTRACES - Goldschmidt Session 10i*

8

9 **Corresponding author**

10 Michael Köbberich, phone: +41 (0) 44 632 07 30, email: michael.koebberich@alumni.ethz.ch

11 **Author affiliations**

12 ¹ Institute of Geochemistry and Petrology, Department of Earth Sciences, ETH Zurich,
13 Clausiusstrasse 25, CH-8092 Zurich, Switzerland

14 **Running head**

15 Ligand controlled Zn isotope fractionation

16 **Keywords**

17 Zinc isotopes, Ligands, Phytoplankton culturing, Metal uptake, GEOTRACES, Trace Metals.

18 **Abstract**

19 The extreme scarcity of zinc (Zn) in the euphotic zone, coupled to deep enrichments, is
20 consistent with biological uptake at the surface and regeneration at depth. In the context of a
21 nutrient-type depth profile so clearly shaped by uptake into phytoplankton, the growing dataset
22 for Zn isotopes presents a challenge. These data either show very minor isotope effects
23 associated with extreme depletion, or enrichment of the light isotopes in the upper ocean. In
24 contrast, culturing of eukaryotes in the laboratory suggests that light Zn isotopes are
25 preferentially taken up into diatoms and coccoliths, implying that Zn depletion at the surface
26 should be associated with extremely heavy residual dissolved signals.

27 Here we present the first Zn isotope measurements for cultured marine cyanobacteria and
28 compare these data to those for eukaryotic diatoms grown under identical conditions. Of the
29 four cyanobacteria cultured, belonging to the genera *Synechococcus* and *Prochlorococcus*,
30 three preferentially take up light Zn into the cell, with a variability that is not fundamentally
31 different between pro- and eukaryotic phytoplankton. We also observe only very subtle
32 differences between Zn/P and Fe/P uptake ratios for these three cyanobacteria groups relative to
33 diatoms grown under the same conditions. A fourth strain exhibits preferential uptake of heavy
34 Zn isotopes, and very high Zn/P ratios. Overall, we speculate that the observed variability
35 among cyanobacteria may be related to the molecular structure of their photosynthetic light
36 harvesting apparatus, adapted to significantly different light niches.

37 These new and published culture data support the hypothesis that cellular $\delta^{66}\text{Zn}$ in culture
38 might largely be controlled by the organic ligands that bind Zn in the medium. Given that the
39 Zn-binding ligands in the ocean have **thermodynamic** stability constants that are orders of
40 magnitude smaller than the EDTA used in culture media, the surprisingly subtle Zn isotope
41 variability in some parts of the surface ocean **may be** reconciled with culture data by the lesser,
42 near zero, preference of these weaker complexes for heavy Zn isotopes.

43

44 **1. Introduction**

45 Intracellular metal quotas (Twining and Baines, 2013; Twining et al., 2003) show that zinc (Zn)
46 and iron (Fe) are the two most abundant trace metals in marine phytoplankton (Morel et al.,
47 2014; Twining and Baines, 2013). Extremely low bioavailable Fe concentrations limit the
48 fixation of atmospheric carbon dioxide (CO₂) by phytoplankton in about 30% of the global
49 surface ocean (Moore et al., 2013), and likely also near the deep chlorophyll maximum of
50 stratified subtropical mid-ocean gyres (Hopkinson and Barbeau, 2008; Sedwick et al., 2005;
51 Sunda and Huntsman, 2015). Although the jury is still out on whether Zn co-limits
52 phytoplankton growth in certain regions of the global ocean (*c.f.* Moore et al., 2013), Zn is
53 often equally, if not more, abundant in the cell than Fe (Twining and Baines, 2013). Both
54 metals serve as co-factors in enzymes of key metabolic pathways. Important examples of Zn
55 containing enzymes are carbonic anhydrases, essential during biomass buildup from reduced
56 carbon (C) and light (Domsic et al., 2008; Morel et al., 2014; Roberts et al., 1997), or alkaline
57 phosphatases for the acquisition of organic phosphorus (P) when phosphate is scarce (Cox and
58 Saito, 2013; Morel et al., 2014; Shaked et al., 2006). Superoxide dismutases can also require
59 sizeable fractions of the cellular Fe and Zn pool, in particular in phototrophs, where light-
60 induced reactions often come with toxic superoxide anions (O₂⁻) that can be reduced by this
61 enzyme (Morel, 2008; Wolfe-Simon et al., 2005). As a result, Zn is extremely scarce in the
62 surface ocean, while the deep ocean is enriched, consistent with biological uptake in the
63 euphotic zone and its regeneration at depth (Bruland, 1980; Bruland et al., 2014).

64 Metal stable isotope data, increasingly available through the international GEOTRACES
65 program, provide a new way of investigating the impact of trace metal availability on
66 phytoplankton growth. However, the data available to date for oceanic Zn isotopes have
67 presented some challenging puzzles. For example, despite drawdown by diatom uptake during
68 northward flow of surface waters, of close to 99% of the Zn upwelled in the Southern Ocean,
69 the Zn-depleted residual water is not shifted to very heavy values (Wang et al., this volume;
70 Zhao et al., 2014), as would be expected for preferential uptake of light isotopes into cells.

71 Furthermore, for nearly all regions outside the Southern Ocean (Conway and John, 2014;
72 Conway and John, 2015; John et al., 2018), dissolved Zn in the upper ocean is significantly
73 enriched in light Zn isotopes compared to the globally rather homogeneous deep ocean. Though
74 Samanta et al. (2017) invoke the uptake of light isotopes with decreased Zn abundances in the
75 surface Tasman Sea, the data are noisy, the correlation is very weak ($r^2 = 0.21$, MSWD = 15)
76 and the fractionation factor implied is within uncertainty of zero. The same very weak
77 relationship and near zero fractionation are seen in the data of Wang et al. (this volume). These
78 findings seem to be at odds with the expectation that light isotopes would be preferentially
79 taken up into cells, and with laboratory culture experiments that find the biomass of marine
80 eukaryotic algae to be enriched in light Zn isotopes with respect to the experimental medium
81 (John and Conway, 2014; John et al., 2007; Köbberich and Vance, 2017; Köbberich and Vance,
82 2018; Samanta et al., 2017).

83 Taxonomic differences among distinct groups of phytoplankton have been considered to drive
84 some of the observed regional and global variability in Zn abundances in the ocean. For
85 example, elevated Zn in diatoms (Twining and Baines, 2013) has been suggested to control
86 Southern Ocean concentrations and, through the water masses advected from it, the pattern of
87 variability in the global ocean (Vance et al., 2017). **On the other hand, it is well-established that**
88 **cellular Zn is closely related to its bioavailability in seawater** (Sunda and Huntsman, 1992),
89 leaving it unclear to what extent changes in the proteome are relevant (Cox and Saito, 2013;
90 Twining and Baines, 2013). Beyond diatoms, Samanta et al. (2017) observed electron transport
91 rates and the photosynthetic efficiency to increase with increasing free Zn^{2+} concentration in
92 another eukaryote, *Emiliania huxleyi*, which was speculated to be due to increased carbonic
93 anhydrase activity.

94 The global biogeography of phytoplankton is such that a great deal of the total chlorophyll
95 belongs to only two major groups of phytoplankton, namely *Synechococcus* or
96 *Prochlorococcus* (Follows and Dutkiewicz, 2010; Follows et al., 2007; Menemenlis et al.,
97 2005). Furthermore, these prokaryotic cyanobacteria are direct descendants of the earliest

98 oxygenic phototrophs, originating during a period of Earth history distinctly different in its
99 ocean chemistry (Falkowski and Knoll, 2007; Knoll et al., 2012; Saito et al., 2003; Sunda and
100 Huntsman, 2015). It has been suggested that this resulted in elevated minimum Fe requirements
101 in prokaryotes, and that this explains their high requirement for Fe relative to eukaryotes in the
102 modern ocean (Brand, 1991; Österberg, 1974; Saito et al., 2003; Sunda and Huntsman, 2015).

103 In the light of these considerations, constraints on how cyanobacteria take up Zn and its
104 isotopes are required. Here we address this requirement. We also present new data for diatoms,
105 cultured under conditions that are as close as possible to those for the cyanobacteria. Our aim is
106 to explore the relative importance of species-dependent differences versus environmental
107 controls for trace metal systematics versus, with implications for the evolution of trace metal
108 requirements in an ocean in which the biology and chemistry have both changed through time.
109 Finally, we consider the emerging dataset for oceanic Zn isotopes in the context of these new
110 constraints, as well as published data, from culture experiments.

111

112 **2. Materials & Methods**

113 Culturing media were prepared either from salts that were of trace metal purity, or from
114 solutions that were cleaned using a chelating resin (Chelex[®] 100, Bio-Rad, USA). All ultrapure
115 water came from a Milli-Q[®] integral water purification system (Merck, Millipore, Germany)
116 with a conductivity of 18.2 MΩ·cm. Reagent grade acids used for preparative purposes were
117 twice purified by sub-boiling distillation before use (DST-1000, Savillex, USA). Handling of
118 all samples and reagents was carried out under “Class 100” clean laboratory conditions at
119 constant humidity of around 10 %, and a temperature of 21.2 ± 0.2 °C.

120 **2.1 Phytoplankton strains**

121 Three different diatoms and four distinct cyanobacteria strains, all axenic, were obtained from
122 the National Center for Marine Algae and Microbiota (NCMA), formerly known as Provasoli-
123 Guillard Center for Culture of Marine Phytoplankton (CCMP), Bigelow Laboratories, USA.

124 Two of the chosen diatoms, *Chaetoceros sp.* (CCMP 199) and *Thalassiosira oceanica* (CCMP
125 1005), originate from oligotrophic surface waters of the Sargasso Sea, North Atlantic. The
126 third, *Thalassiosira weissflogii* (CCMP 1336) came from coastal waters of Long Island Sound,
127 North Atlantic, USA. Three representatives of the genus *Synechococcus* (CCMP 1183, 1334,
128 and 2370, the latter two are also known as WH 7803 and 8102) and *Prochlorococcus marinus*
129 (CCMP 2389, *a.k.a.* MED 4) were chosen to represent the prokaryotic phylum of
130 cyanobacteria. All four prokaryotes are open ocean strains, two of which (CCMP 1334 and
131 2370) originate in the oligotrophic surface waters of the Sargasso Sea, North Atlantic. Sterile
132 techniques were used whenever cultures or media solutions were handled. Axenic conditions
133 were monitored by inspecting small aliquots of stained culture solutions by microscopic
134 methods.

135 An important aim of this contribution is to explore inter-species Zn isotope effects associated
136 with Zn uptake into the cell. Biological fractionation of Zn isotopes during uptake has been
137 related to active transport across the cell membrane (John et al., 2007), a mechanism that for Fe
138 has been shown to be a surface-area related process (Sunda and Huntsman, 1995; Sunda and
139 Huntsman, 1997). The set of species chosen here span the entire size range of pico- and nano-
140 phytoplankton and differ in their surface area to biovolume (A/V) ratio as calculated from their
141 cellular geometry (Fig. 1). The cellular dimensions and geometries of 1362 diatoms (Leblanc et
142 al., 2012) and 181 coccolithophores (O'Brien et al., 2013) came from the MARine Ecosystem
143 DATA (MAREDAT; Buitenhuis et al., 2013) project. Geometric models that are used for
144 calculating cell surface areas and biovolumes (Leblanc et al., 2012; Sun and Liu, 2003) can also
145 be linked to empirical carbon (C) biomass estimates (Leblanc et al., 2012; Smayda, 1978). We
146 use this information to compare our laboratory cultures with the A/V ratios that have previously
147 been considered relevant to natural environments (Fig. 1).

148 **2.2 Culturing techniques**

149 The culturing conditions were similar to Köbberich and Vance (2017). A short summary is
150 given below with the most important differences highlighted. Light was supplied to all

151 phytoplankton cultures in 15- to 9-hour day to night cycles. A constant photon flux density of
152 50 rather than 40 $\mu\text{mol m}^{-2} \text{s}^{-1}$ was used, with one important exception: the high light adapted
153 *Prochlorococcus* strain CCMP 2389 was maintained at 25 $\mu\text{mol m}^{-2} \text{s}^{-1}$, as verified with a
154 newly calibrated spherical quantum sensor LI-193 (LI-COR[®], Nebraska, USA). Cell numbers
155 for calculating specific growth rates were obtained by Coulter counting on a daily basis or by
156 using a hemocytometer, as described in Köbberich and Vance (2017).

157 The artificial culture medium, used here to allow comparison across a range of different
158 eukaryotic and prokaryotic phytoplankton organisms at similar bioavailable Zn^{2+} levels, is
159 similar to that previously reported in Köbberich and Vance (2017). This medium has a seawater
160 base adjusted to a final salinity of about 36 g kg^{-1} . Total ethylenediaminetetraacetic acid
161 (EDTA) concentrations were in the range 95 - 97 $\mu\text{mol l}^{-1}$, and Zn was kept constant to allow
162 inter-species comparison at identical bioavailable Zn. Total Zn concentrations were thus
163 adjusted to obtain free divalent Zn^{2+} and inorganically bound Zn (Zn') levels in the range 67 -
164 72 and 100 - 109 pmol l^{-1} , respectively, for all eukaryotes and *Synechococcus* strains. Aqueous
165 Zn speciation has been calculated following the recommendations of Sunda et al. (2005) and
166 references therein. The artificial seawater medium used to culture the *Prochlorococcus* strain
167 CCMP 2389 had to differ from that used for all other strains for two distinct, though related,
168 reasons. Firstly, *P. marinus* simply does not grow in the above-described broad-spectrum
169 medium. Secondly, to our knowledge, there is currently no recipe available that maintains
170 *Prochlorococcus* as well as all the other species of interest. We thus designed a newly
171 developed medium that mimics the above-described solution as closely as possible, while still
172 achieving sufficient *Prochlorococcus* growth (see Supplementary Information S.1 for further
173 details).

174 All phytoplankton cells were harvested, *i.e.* separated from their residual culturing medium, at
175 or shortly after mid exponential growth, with 0.2 μm filters, using pre-cleaned vertical twin
176 membrane centrifugal concentrators (Vivaspin 20, Sartorius, Germany). Shortly after
177 harvesting, residual media remnants were removed by washing the collected cells with UV-

178 treated equatorial Atlantic seawater, with notably low Zn in the range of 0.01 - 0.05 nmol kg⁻¹
179 (Zhao, 2011). The biomass collected on the filter was re-suspended in pre-cleaned NaCl of
180 seawater osmolality, before the resulting cell suspension was pipetted out of the centrifugal
181 concentrator. After evaporation to dryness, all samples were digested in double distilled 65%
182 HNO₃ at 120 °C for ~16 hours. After a final dry-down, all digested samples were re-dissolved
183 in 2 % HNO₃ for elemental analysis, followed by column chromatography and Zn isotopic
184 analysis (see next section).

185 **2.3 Elemental and stable isotope analysis**

186 The procedures used for elemental and stable isotope analysis are identical to those previously
187 described in Köbberich and Vance (2017) and very similar to those in previous publications
188 from this laboratory (*e.g.*, Little et al., 2016; Vance et al., 2016a; Vance et al., 2016b). In brief,
189 elemental analyses were done on a ThermoScientific Element XRTM inductively-coupled
190 plasma mass spectrometer (ICP-MS). All samples for isotope analysis were purified by anion
191 exchange chromatography (Archer and Vance, 2004; Bermin et al., 2006; Maréchal et al.,
192 1999) and were measured on a Neptune PlusTM multiple-collector inductively-coupled plasma
193 mass spectrometer (MC-ICP-MS) of the same manufacturer. Instrumental mass fractionation,
194 or that occurring during ion exchange chromatography, was corrected using the double spike
195 approach as described by Bermin et al. (2006) and Zhao et al. (2014), in combination with a
196 data reduction scheme presented by Siebert et al. (2001). Procedural blanks were estimated by
197 isotope dilution analysis and are negligible.

198 The data presented here are given in the standard delta notation, in per mil, reported relative to
199 JMC 3-0749 (Maréchal et al., 1999): $\delta^{66}\text{Zn} (\text{‰}) = [({}^{66}\text{Zn}/{}^{64}\text{Zn})_{\text{sample}} / ({}^{66}\text{Zn}/{}^{64}\text{Zn})_{\text{JMC-Lyon}}] - 1$.
200 Accuracy and precision were monitored relative to a secondary standard, IRMM-3702,
201 previously reported to yield a value of +0.32 ‰ (Cloquet et al., 2008; Ponzevera et al., 2006).
202 Relative to JMC-Lyon, we obtain $\delta^{66}\text{Zn} = 0.30 \pm 0.06 \text{ ‰}$ (2 SD, n = 163 over 380 days). All
203 our culturing results are reported as the fractionation observed between the medium and the
204 separated biomass, here denoted $\Delta^{66}\text{Zn} (\text{‰}) = \delta^{66}\text{Zn}_{\text{biomass}} - \delta^{66}\text{Zn}_{\text{medium}}$. Culture experiments

205 were only considered relevant for reporting when nearly 100% of the Zn initially added to the
206 medium was recovered in the residual medium plus the biomass fraction after the experiment,
207 as quantified by isotope dilution. All diagrams plot the external precision, based on replicate
208 analyses of IRMM-3702 as noted above, unless internal errors exceed the external
209 reproducibility.

210 **3. Results**

211 Based on measured growth and metal uptake data, the largest cultured diatom, *T. weissfloggi*,
212 reached Zn uptake rates up to about 26% of the maximum that could be supplied to the cell by
213 diffusion (Table 1). The prokaryotic organisms cultured here were much less likely to be
214 diffusion limited - and consistently contained less than 1% of the amount of Zn that could be
215 supplied by diffusion. Fe exerts a key control on phytoplankton growth and thus metal uptake
216 (Köbberich and Vance, 2017; Sunda and Huntsman, 1995; Sunda and Huntsman, 1997), so that
217 Table 1 also provides data supporting the suggestion that growth is not suppressed as a
218 consequence of diffusion limited Fe supply.

219 Three different diatom strains, each grown on nitrate and urea as the sole N source, were
220 generally found to grow fast, with specific growth rates between 0.65 and 0.77 d⁻¹. At identical
221 irradiance and nutrient levels, three representatives of the genus *Synechococcus* grew at more
222 variable rates, ranging from 0.42 to 0.82 d⁻¹ (Fig. 2A). *Prochlorococcus marinus* – the smallest
223 strain cultured here – grew at a specific growth rate of 0.28 d⁻¹, at half the irradiance level (25
224 μmol m⁻² s⁻¹) applied to all other strains (50 μmol m⁻² s⁻¹).

225 Fe uptake into marine phytoplankton has previously been shown to be a surface area related
226 process (Sunda and Huntsman, 1995; Sunda and Huntsman, 1997). Surface area normalized Fe
227 and Zn uptake rates, calculated from measured cellular quotas and the surface areas shown in
228 Fig. 1, are high and variable for diatoms, reaching up to values that are often greater than 100
229 nmol m⁻² d⁻¹. Those of prokaryotes are mostly much lower (Fig. 2B and C).

230 Carbon or P-normalized cellular Fe and Zn of all measured diatoms are in good agreement with
231 previous culture work (Sunda and Huntsman, 1992; Sunda and Huntsman, 1995) at similar
232 bioavailable metal concentrations. Measured metal to P quotas were converted to Zn/C
233 assuming a Redfield stoichiometry of C:P of 106:1. In good agreement with previous work on a
234 coastal *Synechococcus bacillaris* strain (Sunda and Huntsman, 2015), all studied cyanobacteria
235 yielded higher cellular Fe quotas than the majority of cultured diatoms (Fig. 3A), while their
236 absolute rates of metal transport across the cell membrane were generally found to be very low
237 (Fig. 2B). Except for the *Synechococcus* strain CCMP 2370, the opposite was found for cellular
238 Zn quotas (Fig. 3B), also at comparatively low uptake rates (Fig. 2C). This becomes most
239 apparent if cellular Zn quotas are plotted as a function of Fe quotas (Fig. 3C). Excluding CCMP
240 2370, the highest Zn/P quotas of $\sim 2 \text{ mmol mol}^{-1}$ were found with low Fe/P ratios, while the
241 lowest of $\sim 0.5 \text{ mmol mol}^{-1}$ were reached at Fe/P $\sim 7 \text{ mmol mol}^{-1}$.

242 All the isotope results are given in Table 1. The biomass of the marine diatom *T. oceanica*
243 shows a preference for light isotopes by 0.28‰, similar that previously observed for this strain
244 for a comparable culture medium ($\Delta^{66}\text{Zn}$; John et al., 2007; Köbberich and Vance, 2017).

245 **4. Discussion**

246 Of the two groups of organisms cultured here for Zn isotopes, the data for cyanobacteria are the
247 most novel. Previous studies have presented data for diatoms (John et al., 2007; Köbberich and
248 Vance, 2017; Köbberich and Vance, 2018), while Samanta et al. (2017) have published Zn
249 isotope data for another eukaryote group, the coccoliths. Thus, we first discuss the variation
250 within the cyanobacteria strains cultured, before moving on to compare these new data with the
251 new and published data for eukaryotes.

252 **4.1 Variations in metal uptake characteristics among cyanobacteria**

253 Three of the four cyanobacteria cultured were found to have similar cellular Zn quotas to
254 diatoms, though at the lower end of the latter's range. The opposite is true for cellular Fe quotas
255 (Fig. 3A and 3B), a finding which is in agreement with previous work (Saito et al., 2003; Sunda

256 and Huntsman, 2015; Sunda and Huntsman, 1995). It is also obvious from Fig. 3, that CCMP
257 2370 differs from the other cyanobacteria in its Zn quota. Though this difference is less marked
258 for Fe, it is also the case that the Fe quotas found for CCMP 2370 represent the higher end of
259 the observed spectrum (Fig. 3C). High biomass associated Fe contents might indicate the
260 presence of surface-bound Fe-hydroxides, which could adsorb large quantities of Zn, and this
261 theory might be supported by positive biomass $\Delta^{66}\text{Zn}$ values (see Table 1 and Section 4.3;
262 Gélabert et al., 2006; John et al., 2007). However, the variability in the overall cyanobacterial
263 dataset, for both Fe- and Zn-quotas and including the data for CCMP 2370, is no greater than
264 that seen in natural communities using X-ray fluorescence imaging techniques (Twining and
265 Baines, 2013). Moreover, Tang and Morel (2006) did not detect any increase in cellular Zn/P at
266 the total medium Fe concentrations used here, or for the biomass Fe/P ratios measured here. It
267 is also the case that CCMP 2370 differs from all other cyanobacteria in the greater proportion
268 of phycoerythrin (PE) in its total budget of chromophores (Six et al., 2007). There is,
269 however, currently no known Zn containing enzyme involved in the biosynthesis of PE.
270 Whether the cellular Zn content could be related to such biochemical pathways remains to be
271 addressed in future research (for additional thoughts see section S.5 of the Supplementary
272 Information).

273 **4.2 Similarities and differences between prokaryotic and eukaryotic metal uptake**

274 Culture experiments are performed in a controlled environment. An assessment of taxonomic
275 differences from such experiments is often only possible in terms of whether the phytoplankton
276 of interest is well adapted to the culture conditions used, coupled to a comparison between
277 those culturing conditions and the organism's natural habitat. Thus, despite an extensive body
278 of literature on the physiological response to various types of environmental stress (for a review
279 see Morel et al., 2014) applied in laboratory cultures, it remains challenging to separate purely
280 taxonomic effects from imposed environmental factors.

281 The precise culture conditions chosen here for the eukaryotic organisms were adjusted to yield
282 similar specific growth rates for each organism, using published constraints (Sunda and

283 Huntsman, 1995; Sunda and Huntsman, 1997). Thus, though the open ocean diatom *T.*
284 *oceanica*, as well as a representative of the genus *Chaetoceros*, grew at similar rates for the
285 same Fe', the same growth rates were only achieved for the coastal species, *T. weissflogii*, at Fe'
286 that was almost twice as high (Table 1). Prokaryotes such as the tiny *Prochlorococcus* simply
287 behave too differently to reasonably expect them to yield the same fast growth rates as diatoms
288 in culture (*c.f.* Supplementary Information S.1). In our experiments, CCMP 1183 and 2370
289 were at least close, though somewhat more variable (Fig. 2A).

290 **4.3 Ligand control on $\Delta^{66}\text{Zn}$ recorded in phytoplankton**

291 Based on precautions to avoid diffusion-limited Zn transport towards the cell surface (*c.f.*
292 section S.2 in the Supplementary Information), we can essentially exclude the possibility that
293 any of the negative $\Delta^{66}\text{Zn}$ observed here are likely to be caused by the slightly faster diffusion
294 rates of the lighter ^{64}Zn isotope. Only the cyanobacteria strain CCMP 2370, with unusually high
295 cellular Zn quotas, was found to yield positive $\Delta^{66}\text{Zn}$ values with respect to the bulk culture
296 medium (Fig. 4). All other phytoplankton, whether pro- or eukaryotic, consistently yielded
297 negative $\Delta^{66}\text{Zn}$ values (Table 1). These findings are in good agreement with previous culture
298 experiments (John et al., 2007; Köbberich and Vance, 2017; Samanta et al., 2017), at similar
299 bioavailable Zn levels, as illustrated in Fig. 5.

300 The equilibrium fractionation between Zn-EDTA and 'free' Zn is such that heavy Zn isotopes
301 are preferentially bound to the organic chelator (Ban et al., 2002; Ding et al., 2010a; Ding et al.,
302 2010b; Markovic et al., 2017), while the bioavailable Zn^{2+} pool is enriched in light Zn isotopes
303 - before any interaction with phytoplankton. In agreement with the suggestion of John et al.
304 (2007), we thus argue that a substantial portion of the observed $\Delta^{66}\text{Zn}$ in cultured
305 phytoplankton is actually the result of this equilibrium fractionation in the medium, rather than
306 resulting from biological uptake. Although there is strain-dependent variability in the extent to
307 which the light Zn isotope is taken up into phytoplankton, there are no systematic differences
308 between cyanobacteria and diatoms. In fact, excluding CCMP 2370, the absolute ranges
309 observed among different representatives of both clades are almost indistinguishable from each

310 other. Neither absolute rates of Zn transport across the cell surface area, nor A/V ratios (see
311 Supplementary Information, Fig. S.1), seem to correlate with the extent to which light Zn
312 isotopes are preferentially taken up. This could simply be due to the fact that the studied
313 diversity is still too small, obscuring any potential pattern. On the other hand, the uptake
314 mechanism may be important, given that there is an increasing preference for light Zn isotopes
315 as a result of additional active transport across the cell wall beyond the level associated with
316 high-affinity transporters alone (John et al., 2007). Thus, the observed variability might be
317 caused by the fact that the onset of low-affinity Zn uptake may occur at different bioavailable
318 Zn concentrations, as previously identified for *T. oceanica* (John et al., 2007) and *Emiliania*
319 *huxleyi* (Samanta et al., 2017). In this study, bioavailable Zn was chosen to be at the higher end
320 of the range previously considered relevant for high-affinity uptake (for a more detailed
321 discussion, see Köbberich and Vance, 2017). Thus, it is possible that light signatures seen in
322 some of the strains studied here might be explained by isotope fractionation associated with
323 active low-affinity transporters superimposed on a fractionation caused by the high-affinity
324 mechanism.

325 **5. Conclusion and oceanic implications**

326 The two first order features of the oceanic distributions of Zn isotopes that are emerging as data
327 accumulates are: 1) in the Southern Ocean, despite often dramatic drawdown of Zn at the
328 surface, mostly by diatoms, variations in the small residual Zn pool are very muted (*e.g.*, Wang
329 et al., this volume; Zhao et al., 2014); 2) outside the Southern Ocean, residual seawater tends to
330 be lighter in the upper ocean, seeming to imply the uptake of heavy isotopes (*e.g.*, Conway and
331 John, 2014), though where high depth resolution is available near the surface it is often the case
332 that these light values actually occur in the immediate sub-surface (*e.g.*, Wang et al., this
333 volume). Though variations in dissolved Zn isotopes in the surface Southern Ocean are indeed
334 muted, there is also a slight minimum at 100-200m (Wang et al., this volume). The above
335 observations are both, at first glance, inconsistent with the finding of light Zn isotopes in

336 phytoplankton cells in culture. Here we discuss each of the above observations of the real ocean
337 in turn, in the context of the summary of culturing experiments in Fig. 5.

338 An important conclusion from Fig. 5 is that a large proportion of the enrichment of light Zn in a
339 variety of studied pro- and eukaryotic phytoplankton can be explained by the presence of
340 organic ligands in culture media. Consistent with a postulate by John et al. (2007), heavy Zn
341 isotopes are preferentially bound to the trace metal buffer EDTA in culture media, while the
342 'free' bioavailable Zn pool is already enriched in light isotopes before uptake. A significant
343 proportion of light Zn found in phytoplankton after a culture experiment might thus be the
344 result of an aqueous equilibrium in seawater, rather than the consequence of kinetic isotope
345 fractionation during active transport across the cell wall. Although the uncertainty on the
346 isotope fractionation associated with the relevant Zn-EDTA equilibrium is still large (Ban et al.,
347 2002; Ding et al., 2010a; Ding et al., 2010b; Markovic et al., 2017), kinetic isotope effects
348 associated with uptake are only rarely outside the range that could be explained by the presence
349 of this strong ligand.

350 One could argue that, since the real ocean also contains strong ligands that bind Zn, it is still the
351 $\Delta^{66}\text{Zn}$ fractionation with respect to bulk medium that is the most relevant for the great majority
352 of oceanic regimes. For example, Ellwood and Van den Berg (2000) have shown that 94 - 99%
353 of all Zn in the open NE Atlantic is bound to strong organic complexes. Free Zn concentrations
354 - at 6 - 20 pmol l⁻¹ - in those regions are low, but not low enough to limit the growth of a typical
355 oceanic species (Ellwood and Van den Berg, 2000). Thus, the situation regarding complexation
356 of Zn in the real ocean is *qualitatively* analogous to that in culture experiments, with the
357 bioavailable pool being lighter than the ligand bound fraction.

358 In the surface Southern Ocean, Zn is rapidly drawn down by diatom uptake, by almost 2 orders
359 of magnitude relative to the upwelled deep waters (*e.g.*, Vance et al., 2017; Zhao et al., 2014).
360 If such uptake prefers the light isotope to the extent seen for $\Delta^{66}\text{Zn}_{\text{biomass} - \text{bulk medium}}$ in culturing
361 experiments (Fig. 5), then the $\delta^{66}\text{Zn}$ of the residual Zn-depleted water should exceed 1‰, when
362 in fact it barely rises above the deep ocean average $\delta^{66}\text{Zn}$ of +0.5‰ more than analytical

363 uncertainty (Wang et al., this volume; Zhao et al., 2014). We suggest that the answer to this
364 conundrum lies in the positive relationship, observed by Markovic et al. (2017) in experiment,
365 between the degree of isotope separation between free Zn^{2+} and the organically bound complex
366 and the strength of that complex. Given that the conditional stability constants of Zn binding by
367 organic complexation in the real ocean are about 6 orders of magnitude lower than those for
368 EDTA (e.g., Ellwood and Van den Berg, 2000; Markovic et al., 2017), and given the
369 relationship observed in Markovic et al. (2017), it may actually be no surprise that the real
370 oceanic data often show more subtle isotope effects than cultures. It could be that the answer to
371 this problem originates with differences in the speciation of Zn in culture versus seawater.
372 Markovic et al. (2017) present experimental findings showing that isotope fractionation
373 between free Zn and the organically-bound complex depends on the thermodynamic stability
374 constant for that complex, which for EDTA is about 6 orders of magnitude greater than those
375 for Zn in the real ocean (e.g., Bruland, 1989; Ellwood and van den Berg, 2000; Markovic et al.,
376 2017). However, Bruland (1989) also showed that the *conditional* stability constant for Zn-
377 EDTA complexes in seawater are lower than those for natural organic ligands, due to side
378 reactions between EDTA and Ca and Mg ions that do not occur for the natural ligands (Bruland
379 et al., 1989).

380 Finally, we turn to the apparently light Zn isotope values in areas outside the Southern Ocean,
381 implying loss of *heavy* isotopes during Zn drawdown. John and Conway (2014) have suggested
382 an explanation in terms of scavenging to particulate organic matter (John and Conway, 2014).
383 One issue with this suggestion is that the experiment in which scavenging, and Zn isotope
384 fractionation associated with it, was observed (John and Conway, 2014) contained none of the
385 organic ligands that stabilize Zn in solution, whereas most of the surface ocean contains more
386 than 10 times more Zn-specific ligands than total dissolved Zn found in the NE Atlantic
387 (Ellwood and Van den Berg, 2000). The one part of the surface ocean where this is known not
388 to be the case is the Southern Ocean, (Baars and Croot, 2011), and this is where heavy surface
389 isotopes are not seen.

390 ~~As shown in the data compilation in Wang et al. (this Volume), most profiles with generally~~
391 ~~negative $\delta^{66}\text{Zn}$ in the upper ocean actually feature a heavy value right at the surface. In at least~~
392 ~~some cases, this upward move to heavy Zn isotopes is defined by more than a single sample.~~
393 ~~We suggest, therefore, that there may, in fact, be uptake of slightly light isotopes at the surface~~
394 ~~and that the light isotopes that apparently dominate the upper ocean in e.g. the North Atlantic~~
395 ~~(Conway and John, 2014) are the result of very shallow sub-surface (peaking at about 100 m~~
396 ~~but extending down to 500 m) regeneration of biomass associated light Zn isotopes (e.g.,~~
397 ~~Bermin et al., 2006). In this view, the data from the surface ocean is also not actually~~
398 ~~inconsistent with culture experiments that suggest slight preferential uptake of light isotopes~~
399 ~~into phytoplankton (Fig. 5). Such a hypothesis does require that Zn cycling up and down~~
400 ~~between the photic zone and the immediate sub-surface must, outside the Southern Ocean, be to~~
401 ~~a large extent decoupled from the deep ocean underneath. In this view, consistent with the~~
402 ~~behavior of other nutrients in the ocean, Zn behavior is split by a Southern Ocean~~
403 ~~biogeochemical divide (e.g., Marinov et al., 2006; Sarmiento et al., 2004; Vance et al., 2017),~~
404 ~~with a Zn rich deep cycle fed by deep waters from the Southern Ocean, and that only re-~~
405 ~~connects to the surface in the Southern Ocean, below a rather isolated extra-Southern shallow~~
406 ~~ocean that is fed by the Zn poor upper ocean water masses advected out of the Southern Ocean.~~

407 Finally, we turn to the apparently light Zn isotope values in areas outside the Southern Ocean.
408 John and Conway (2014) have suggested an explanation in terms of preferential loss of heavy
409 isotope through scavenging to particulate organic matter. One issue with this suggestion is that
410 the experiment in which scavenging, and Zn isotope fractionation associated with it, was
411 observed (John and Conway, 2014) contained none of the organic ligands that stabilize Zn in
412 solution, whereas most of the surface ocean contains more than 10 times more Zn-specific
413 ligands than total dissolved Zn found in the NE Atlantic (Ellwood and Van den Berg, 2000).
414 The one part of the surface ocean where this is known not to be the case is the Southern Ocean,
415 (Baars and Croot, 2011), and this is where heavy surface isotopes are not seen.

416 As shown in the data compilation in Wang et al. (this volume), most profiles with generally
417 negative $\delta^{66}\text{Zn}$ in the upper ocean actually feature a heavy value right at the surface. In at least
418 some cases, this upward move to heavy Zn isotopes is defined by more than a single sample.
419 We suggest, therefore, that the data are often consistent with uptake of slightly light isotopes at
420 the surface and that the light isotopes that apparently dominate the upper ocean in *e.g.* the
421 North Atlantic (Conway and John, 2014) are at least partially the result of very shallow sub-
422 surface (peaking at about 100 m but extending down to 500 m) regeneration of biomass-
423 associated light Zn isotopes (*e.g.*, Bermin et al., 2006). It is also clear, however, that mass
424 balance considerations mean that such a process cannot explain the overall light upper layer
425 outside the Southern Ocean - *i.e.* the upper 500m. This Southern Ocean biogeochemical divide
426 is emerging as a key feature of the ocean biogeochemistry of Zn, consistent with the behavior
427 of other nutrients in the ocean (*e.g.*, Marinov et al., 2006; Sarmiento et al., 2004; Vance et al.,
428 2017). The Zn-rich deep cycle is fed by deep waters that only re-connect to the surface in the
429 Southern Ocean, and sits below a rather isolated extra-Southern shallow ocean exhibiting
430 different processes. Recent studies have highlighted a very similar pattern for Cd and its
431 isotopes, with Cd isotopes apparently buffered to a surprisingly constant value in this low-
432 latitude surface pool (*e.g.*, Xie et al., 2017; Sieber et al., this volume). It is speculation at
433 present, but the idea that one of the processes that have been invoked for Cd, supply from the
434 atmosphere (Xie et al., 2017), could also explain light Zn in the low latitude surface merits
435 further investigation.

436 **Acknowledgements**

437 We are grateful to Alysia D. Cox for help with setting up a phytoplankton culturing lab at ETH
438 Zurich and to Timothy I. Eglinton for allowing us access to biology laboratories and incubator
439 facilities. We also wish to thank Corey Archer for valuable support with elemental and isotopic
440 analysis and Amélie Ritscher for her work as a research assistant at ETH Zurich. Financial
441 support was provided by ETH and the Swiss National Science Foundation (SNF) through grant
442 200021-143262.

443 **References**

- 444 Archer, C., Vance, D., 2004. Mass discrimination correction in multiple-collector plasma
445 source mass spectrometry: an example using Cu and Zn isotopes. *Journal of Analytical*
446 *Atomic Spectrometry*, 19: 656-665.
- 447
448 Baars, O., Croot, P.L., 2011. The speciation of dissolved zinc in the Atlantic sector of the
449 Southern Ocean. *Deep Sea Research Part II: Topical Studies in Oceanography*, 58:
450 2720-2732.
- 451
452 Ban, Y., Aida, M., Nomura, M., Fujii, Y., 2002. Zinc isotope separation by ligand exchange
453 chromatography using cation exchange resin. *Journal of Ion Exchange*, 13: 46-52.
- 454
455 Bermin, J., Vance, D., Archer, C., Statham, P.J., 2006. The determination of the isotopic
456 composition of Cu and Zn in seawater. *Chemical Geology*, 226: 280-297.
- 457
458 Brand, L.E., 1991. Minimum iron requirements of marine phytoplankton and the implications
459 for the biogeochemical control of new production. *Limnology and Oceanography*, 36:
460 1756-1771.
- 461
462 Bruland, K.W., 1980. Oceanographic distributions of cadmium, zinc, nickel, and copper in the
463 North Pacific Earth and Planetary Science Letters, 47: 176-198.
- 464
465 **Bruland, K.W. (1989) Complexation of zinc by natural organic ligands in the central North**
466 **Pacific. *Limnology and Oceanography* 34: 269-285.**
- 467
468 Bruland, K.W., Middag, R., Lohan, M.C., 2014. Controls of trace metals in seawater. In:
469 Heinrich, D.H., Karl, K.T. (Eds.), *Treatise on Geochemistry*. Elsevier, Oxford, pp. 19-
470 51.
- 471
472 Buitenhuis, E.T. et al., 2013. MAREDAT: towards a world atlas of MARine Ecosystem DATA.
473 *Earth System Science Data*, 5: 227-239.
- 474
475 Cloquet, C., Carignan, J., Lehmann, M., Vanhaecke, F., 2008. Variation in the isotopic
476 composition of zinc in the natural environment and the use of zinc isotopes in
477 biogeosciences: a review. *Analytical and Bioanalytical Chemistry*, 390: 451-463.
- 478
479 Conway, T.M., John, S.G., 2014. The biogeochemical cycling of zinc and zinc isotopes in the
480 North Atlantic Ocean. *Global Biogeochemical Cycles*, 28: 1111-1128.
- 481
482 Conway, T.M., John, S.G., 2015. The cycling of iron, zinc and cadmium in the North East
483 Pacific Ocean – insights from stable isotopes. *Geochimica et Cosmochimica Acta*, 164:
484 262-283.
- 485
486 Cox, A.D., Saito, M.A., 2013. Proteomic responses of oceanic *Synechococcus* WH8102 to
487 phosphate and zinc scarcity and cadmium additions. *Frontiers in Microbiology*, 4: 387,
488 pp. 1-17.

489
490 Ding, X., Nomura, M., Fujii, Y., 2010a. Zinc isotope effects by chromatographic chelating
491 exchange resin. *Progress in Nuclear Energy*, 52: 164-167.

492
493 Ding, X., Nomura, M., Suzuki, T., Fujii, Y., 2010b. Chromatographic zinc isotope separation
494 by chelating exchange resin. *Chromatographia*, 71: 195-199.

495
496 Domsic, J.F. et al., 2008. Entrapment of Carbon Dioxide in the Active Site of Carbonic
497 Anhydrase II. *Journal of Biological Chemistry*, 283: 30766-30771.

498
499 Ellwood, M.J., Van den Berg, C.M.G., 2000. Zinc speciation in the Northeastern Atlantic
500 Ocean. *Marine Chemistry*, 68: 295-306.

501
502 Falkowski, P.G., Knoll, A.H., 2007. *Evolution of primary producers in the sea*. Elsevier
503 Academic Press.

504
505 Follows, M.J., Dutkiewicz, S., Grant, S., Chisholm, S.W., 2007. Emergent Biogeography of
506 Microbial Communities in a Model Ocean. *Science*, 315: 1843-1846.

507
508 Follows, M.J., Dutkiewicz, S., 2010. Modeling Diverse Communities of Marine Microbes.
509 *Annual Review of Marine Science*, 3: 427-451.

510
511 Gélabert, A. et al., 2006. Interaction between zinc and freshwater and marine diatom species:
512 surface complexation and Zn isotope fractionation. *Geochimica et Cosmochimica Acta*,
513 70: 839-857.

514
515 Hopkinson, B.M., Barbeau, K.A., 2008. Interactive influences of iron and light limitation on
516 phytoplankton at subsurface chlorophyll maxima in the eastern North Pacific.
517 *Limnology and Oceanography*, 53: 1303-1318.

518
519 John, S.G., Geis, R.W., Saito, M.A., Boyle, E.A., 2007. Zinc isotope fractionation during high-
520 affinity and low-affinity zinc transport by the marine diatom *Thalassiosira oceanica*.
521 *Limnology and Oceanography*, 52: 2710-2714.

522
523 John, S.G., Conway, T.M., 2014. A role for scavenging in the marine biogeochemical cycling
524 of zinc and zinc isotopes. *Earth and Planetary Science Letters*, 394: 159-167.

525
526 John, S.G., Helgoe, J., Townsend, E., 2018. Biogeochemical cycling of Zn and Cd and their
527 stable isotopes in the Eastern Tropical South Pacific. *Marine Chemistry* 201: 256-262.

528
529 Knoll, A.H., Canfield, D.E., Konhauser, K.O. (Eds.), 2012. *Fundamentals of Geobiology*. John
530 Wiley & Sons, Ltd., pp. 443.

531
532 Köbberich, M., Vance, D., 2017. Kinetic control on Zn isotope signatures recorded in marine
533 diatoms. *Geochimica et Cosmochimica Acta*, 210: 97-113.

534

535 Köbberich, M., Vance, D., 2018. Zinc association with surface-bound iron-hydroxides on
536 cultured marine diatoms: A zinc stable isotope perspective. *Marine Chemistry*.

537
538 Leblanc, K. et al., 2012. A global diatom database – abundance, biovolume and biomass in the
539 world ocean. *Earth System Science Data*, 4: 149-165.

540
541 Little, S.H., Vance, D., McManus, J., Severmann, S., 2016. Key role of continental margin
542 sediments in the oceanic mass balance of Zn and Zn isotopes. *Geology*, 44: 207-210.

543
544 Maréchal, C.N., Télouk, P., Albarède, F., 1999. Precise analysis of copper and zinc isotopic
545 compositions by plasma-source mass spectrometry. *Chemical Geology*, 156: 251-273.

546
547 Marinov, I., Gnanadesikan, A., Toggweiler, J.R., Sarmiento, J.L., 2006. The Southern Ocean
548 biogeochemical divide. *Nature*, 441: 964-967.

549
550 Markovic, T. et al., 2017. Experimental determination of zinc isotope fractionation in
551 complexes with the phytosiderophore 2'-deoxymugeneic acid (DMA) and its structural
552 analogues, and implications for plant uptake mechanisms. *Environmental Science &*
553 *Technology*, 51: 98–107.

554
555 Menemenlis, D. et al., 2005. NASA supercomputer improves prospects for ocean climate
556 research. *Eos, Transactions American Geophysical Union*, 86: 89-96.

557
558 Moore, C.M. et al., 2013. Processes and patterns of oceanic nutrient limitation. *Nature*
559 *Geoscience*, 6: 701-710.

560
561 Morel, F.M.M., 2008. The co-evolution of phytoplankton and trace element cycles in the
562 oceans. *Geobiology*, 6: 318-324.

563
564 Morel, F.M.M., Milligan, A.J., Saito, M.A., 2014. Marine bioinorganic chemistry: the role of
565 trace metals in the oceanic cycles of major nutrients. In: Heinrich, D.H., Karl, K.T.
566 (Eds.), *Treatise on Geochemistry*. Elsevier, Oxford, pp. 123-150.

567
568 O'Brien, C.J. et al., 2013. Global marine plankton functional type biomass distributions:
569 coccolithophores. *Earth System Science Data*, 5: 259-276.

570
571 Österberg, R., 1974. Origins of metal ions in biology. *Nature*, 249: 382-383.

572
573 Ponzevera, E. et al., 2006. Mass discrimination during MC-ICPMS isotopic ratio
574 measurements: investigation by means of synthetic isotopic mixtures (IRMM-007
575 series) and application to the calibration of natural-like zinc materials (Including
576 IRMM-3702 and IRMM-651). *Journal of the American Society for Mass Spectrometry*,
577 17: 1413-1428.

578
579 Roberts, S.B., Lane, T.W., Morel, F.M.M., 1997. Carbonic anhydrase in the marine diatom
580 *Thalassiosira weissflogii* (Bacillariophyceae). *Journal of Phycology*, 33: 845-850.

581

582 Saito, M.A., Sigman, D.M., Morel, F.M.M., 2003. The bioinorganic chemistry of the ancient
583 ocean: the co-evolution of cyanobacterial metal requirements and biogeochemical
584 cycles at the Archean–Proterozoic boundary? *Inorganica Chimica Acta*, 356: 308-318.
585

586 Samanta, M., Ellwood, M.J., Sinoir M., Hassler C.S., 2017. Dissolved zinc isotope cycling in
587 the Tasman Sea, SW Pacific Ocean. *Marine Chemistry*: 192: 1-12.
588

589 Samanta, M., Ellwood, M.J., Strzepek, R.F., 2017. Zinc isotope fractionation by *Emiliana*
590 *huxleyi* cultured across a range of free zinc ion concentrations. *Limnology and*
591 *Oceanography*: 63: 660-671.
592

593 Sarmiento, J.L., Gruber, N., Brzezinski, M.A., Dunne, J.P., 2004. High-latitude controls of
594 thermocline nutrients and low latitude biological productivity. *Nature*, 427: 56-60.
595

596 Sedwick, P.N., Church, T.M., Bowie, A.R., Marsay, C.M., Ussher, S.J., Achilles, K.M.,
597 Lethaby, P.J., Johnson, R.J., Sarin, M.M., McGillicuddy, D.J. (2005), Iron in the
598 Sargasso Sea (Bermuda Atlantic Time-series Study region) during summer: Eolian
599 imprint, spatiotemporal variability, and ecological implications, *Global*
600 *Biogeochemical Cycles*, 19, GB4006.
601

602 Shaked, Y., Xu, Y., Leblanc, K., Morel, F.M.M., 2006. Zinc availability and alkaline
603 phosphatase activity in *Emiliana huxleyi*: Implications for Zn-P co-limitation in the
604 ocean. *Limnology and Oceanography*, 51: 299-309.
605

606 Sieber, M., Conway, T.M., de Souza, G.F., Obata, H., Takano, S., Sohrin, Y., Vance, D., in
607 press. Physical and biogeochemical controls on the distribution of dissolved cadmium
608 and its isotopes in the Southwest Pacific Ocean. *Chemical Geology*, this volume.
609

610 Siebert, C., Nägler, T.F., Kramers, J.D., 2001. Determination of molybdenum isotope
611 fractionation by double-spike multicollector inductively coupled plasma mass
612 spectrometry. *Geochemistry, Geophysics, Geosystems*, 2: 1032.
613

614 Six, C. et al., 2007. Diversity and evolution of phycobilisomes in marine *Synechococcus spp.*: a
615 comparative genomics study. *Genome Biology*, 8: R259 pp. 1-22.
616

617 Smayda, T.J., 1978. From phytoplankters to biomass. In: Sournia, A. (Ed.), *Phytoplankton*
618 *manual*. Museum National d'Histoire Naturelle, Paris, pp. 273-279.
619

620 Sun, J., Liu, D., 2003. Geometric models for calculating cell biovolume and surface area for
621 phytoplankton. *Journal of Plankton Research*, 25: 1331-1346.
622

623 Sunda, W.G., Huntsman, S.A., 1992. Feedback interactions between zinc and phytoplankton in
624 seawater. *Limnology and Oceanography*, 37: 25-40.
625

626 Sunda, W.G., Huntsman, S.A., 1995. Iron uptake and growth limitation in oceanic and coastal
627 phytoplankton. *Marine Chemistry*, 50: 189-206.
628

629 Sunda, W.G., Huntsman, S.A., 1997. Interrelated influence of iron, light and cell size on marine
630 phytoplankton growth. *Nature*, 390: 389-392.

631

632 Sunda, W.G., Price, N.M., Morel, F.M.M., 2005. Trace metal ion buffers and their use in
633 culture studies. In: Andersen, R.A. (Ed.), *Algal Culturing Techniques*. Academic Press,
634 Burlington.

635

636 Sunda, W., Huntsman, S., 2015. High iron requirement for growth, photosynthesis, and low-
637 light acclimation in the coastal cyanobacterium *Synechococcus bacillaris*. *Frontiers in*
638 *Microbiology*, 6: 561.

639

640 Tang, D., Morel, F.M.M., 2006. Distinguishing between cellular and Fe-oxide-associated trace
641 elements in phytoplankton. *Marine Chemistry*, 98: 18-30.

642

643 Twining, B.S. et al., 2003. Quantifying trace elements in individual aquatic protist cells with a
644 synchrotron X-ray fluorescence microprobe. *Analytical Chemistry*, 75: 3806-3816.

645

646 Twining, B.S., Baines, S.B., 2013. The trace metal composition of marine phytoplankton.
647 *Annual Review of Marine Science*, 5: 191-215.

648

649 Vance, D. et al., 2016a. The oceanic budgets of nickel and zinc isotopes: the importance of
650 sulfidic environments as illustrated by the Black Sea. *Philosophical Transactions of the*
651 *Royal Society A: Mathematical, Physical and Engineering Sciences*, 374: 1-26.

652

653 Vance, D. et al., 2016b. The behaviour of Cu and Zn isotopes during soil development: controls
654 on the dissolved load of rivers. *Chemical Geology*, 445: 36-53.

655

656 Vance, D. et al., 2017. Silicon and zinc biogeochemical cycles coupled through the Southern
657 Ocean. *Nature Geoscience*, 10: 202-206.

658

659 Wang, R.M., Archer, C., Bowie, A.R., Vance, D., in press. Zinc and nickel isotopes in seawater
660 from the Indian Sector of the Southern Ocean: the impact of natural iron fertilization
661 versus Southern Ocean hydrography and biogeochemistry. *Chemical Geology*, this
662 volume.

663

664 Wolfe-Simon, F., Grzebyk, D., Schofield, O., Falkowski, P.G., 2005. The role and evolution of
665 superoxide dismutases in algae. *Journal of Phycology*, 41: 453-465.

666

667 Xie, R.C., Galer, S.J.G., Abouchami, W., Rijkenberg, M.J.A., de Baar, H.J.W., De Jong, J.,
668 Andreae, M.O., 2017. Non-Rayleigh control of upper-ocean Cd isotope fractionation in
669 the western South Atlantic, *Earth and Planetary Science Letters*, 471: 94-103.

670

671 Zhao, Y., 2011. The carbon cycle and bioactive trace metals in the oceans: constraints from
672 zinc isotopes. Dissertation, University of Bristol.

673

674 Zhao, Y., Vance, D., Abouchami, W., de Baar, H.J.W., 2014. Biogeochemical cycling of zinc
675 and its isotopes in the Southern Ocean. *Geochimica et Cosmochimica Acta*, 125: 653-
676 672.
677

678 **Figure captions**

679 *full page: Table 1.* Measured Fe and Zn uptake rates, cellular quotas, use efficiencies, and Zn
680 isotope results ($\Delta^{66}\text{Zn}_{\text{biomass} - \text{medium}} = \delta^{66}\text{Zn}_{\text{biomass}} - \delta^{66}\text{Zn}_{\text{medium}}$).

681 *two-column fitting image: Fig. 1.* Comparison of surface area to biovolume (A/V) ratios for all
682 phytoplankton cultured here to the ranges observed in natural communities as derived from
683 MARine Ecosystem DATa (MAREDAT; Buitenhuis et al., 2013).

684 *single-column fitting image: Fig. 2.* Specific growth and metal uptake rates as a function of
685 A/V ratios for all cultured diatoms and cyanobacteria.

686 *single-column fitting image: Fig. 3.* Cellular Fe and Zn quotas as a function of A/V ratios (A
687 and B) and their interdependency (C) for all cultured diatoms and cyanobacteria.

688 *single-column fitting image: Fig. 4.* $\Delta^{66}\text{Zn}$ fractionation of cyanobacteria, which are variably
689 well adapted to the applied nutrient and light conditions as a result of their different light
690 harvesting strategies.

691 *two-column fitting image: Fig. 5.* Comparison of the Zn isotope fractionation upon uptake for
692 all phytoplankton studied here, along with data from the literature. The red band indicates the
693 range of $\Delta^{66}\text{Zn}$ values that could be explained simply by the presence of EDTA as a strong
694 organic chelator in the culture medium, and published data for Zn isotope separation between
695 Zn-EDTA and Zn^{2+} (Ban et al., 2002; Ding et al., 2010a; Ding et al., 2010b; Markovic et al.,
696 2017).

1

2

Supplementary Information

3

Associated with:

4

Zn isotope fractionation during uptake into

5

marine phytoplankton: implications for

6

oceanic zinc isotopes

7

Michael Köbberich^{1*} and Derek Vance¹

8

*To whom correspondence should be addressed

9

Submitted to: *Chemical Geology*

10

Special issue: *GEOTRACES - Goldschmidt Session 10i*

11

12 **S.1 A novel artificial *Prochlorococcus* medium**

13 In common with previous work (Anderson et al., 1978; Berges et al., 2001; Harrison et al.,
14 1990; Morel et al., 1979; Price et al., 1989; Sunda et al., 2005), the strong chelating agent,
15 EDTA, was used to maintain constant and low bioavailable Zn levels over the course of all
16 culture experiments conducted here. The use of constant EDTA concentrations (at around 100
17 $\mu\text{mol l}^{-1}$) simplifies not only inter-species comparison but also direct comparison with
18 published work. From a Zn stable isotope perspective, EDTA has previously been suggested to
19 drive the bioavailable metal pool towards lighter isotope compositions, as heavy Zn isotopes
20 are preferentially associated with the chelating agent (John et al., 2007; Köbberich and Vance,
21 2017). Since the addition of any organic compound bears the risk of affecting the isotopic
22 composition of bioavailable Zn, we sought to avoid natural seawater bases and to keep EDTA
23 high (at around 100 $\mu\text{mol l}^{-1}$; Sunda et al., 2005) and as close to constant as possible, to avoid
24 further complications potentially caused by the distribution of Zn isotopes among aqueous
25 species. All media previously used for culturing *Prochlorococcus* (Chisholm, 1992; Laloui et
26 al., 2002; Moore et al., 2007; Moore et al., 1998; Rippka et al., 2000) have furthermore
27 involved EDTA concentrations a factor of 8 lower than this. In brief, the artificial
28 *Prochlorococcus* medium used here differs from that used for the other organisms cultured here
29 in the following key features: its nitrogen (N) source, total molybdenum and selenium
30 concentrations, its trace metal buffer capacity, and consequently the bioavailable concentrations
31 of all divalent metals.

32 As none of the currently known isolates has been reported to grow on nitrate, N was supplied as
33 ammonia, by means of ammonium chloride salt, adjusted to yield a final concentration of 538
34 $\mu\text{mol l}^{-1}$. Analogous to the widely used enriched natural seawater PRO99 (Moore et al., 2007;
35 Moore et al., 2002), total molybdenum (Mo) and selenium (Se) concentrations were set to
36 elevated – for culture media – levels of 3 and 10 nmol l^{-1} , respectively. In contrast to PRO99,
37 but identical to the broad-spectrum medium used for the other organisms (Section 2.1), Mo
38 stock solutions were prepared with Na_2MoO_4 , while those of Se were made from a hydrated

39 $\text{Na}_2\text{SeO}_3 \cdot 5 \text{H}_2\text{O}$ salt. Given increased EDTA concentrations of $100 \mu\text{mol l}^{-1}$, while total
40 concentrations of all divalent cations in PRO99 remain unmodified, the non-complexed
41 bioavailable metal fraction would be lowered. In a series of preliminary experiments, we found
42 that this increased degree of trace metal buffering by EDTA caused insufficient
43 *Prochlorococcus* growth, pointing to the need to adapt the overall trace metal balance. The total
44 concentrations of the transition metals iron (Fe), cobalt (Co), nickel (Ni), and copper (Cu) were
45 therefore adjusted to yield Me' levels of about 250, 100, 50, and 0.5 pmol l^{-1} , respectively. The
46 abundance of Zn' at the given EDTA content is 138 pmol l^{-1} and that of Zn^{2+} 91 pmol l^{-1} .
47 Growth rates of the cultured *Prochlorococcus* were found to be low compared to values for this
48 clone in Moore and Chisholm (1999), who also report the optimum light level for this clone to
49 be around $100 \mu\text{mol photons m}^{-2} \text{ s}^{-1}$. Here we observed maximum growth at much lower light
50 levels of $< 30 \mu\text{mol photons m}^{-2} \text{ s}^{-1}$ with insignificant growth at $50 \mu\text{mol photons m}^{-2} \text{ s}^{-1}$. The
51 observed difference is likely to be caused by the use of a fundamentally different synthetic
52 seawater solution. For example, Moore and Chisholm (1999) enriched natural seawater with
53 nutrients.

54 **S.2 Diffusion limitation: Theory & Calculation**

55 Resource supply to a phytoplankton cell becomes diffusion limited as soon as the cellular
56 uptake rate of that resource exceeds the maximum rate of supply via diffusion through the
57 medium. Early work noted that large diatoms (small surface area / biovolume ratios, *c.f.* Fig.
58 S.1A) are often more prone to becoming diffusion limited, in cultures with identical
59 bioavailable Zn concentrations, than much smaller cells (Sunda and Huntsman, 1992). Light
60 isotopes of Zn have been shown experimentally to diffuse slightly faster than heavier isotopes
61 (Rodushkin et al., 2004), a process that could potentially lead to the enrichment of the light
62 isotopes of Zn in phytoplankton cells (John et al., 2007; Samanta et al., 2017). Given that the
63 aim of this study is to compare different sized phytoplankton with respect to Zn isotope effects
64 associated with the specific process of cellular uptake, rather than as a result of diffusion-
65 induced gradients in the medium, it becomes important to prevent diffusion limitation in all

66 cultures prepared for comparison. It was, thus necessary to identify a set of culturing conditions
67 that allows comparison of the widest possible range of differently sized phytoplankton whilst
68 ensuring that the Zn isotope composition of the diffusion limitation does not occur across the
69 size range.

70 Whether an individual cell becomes diffusion limited depends on a range of parameters: cell
71 size but also the ambient Zn' level, the specific growth rate (μ), and the amount of Zn taken up
72 per cell (as recorded *e.g.* by cellular Zn/P ratios). The cellular dimension and geometries of
73 MAREDAT diatoms (Leblanc et al., 2012) and coccolithophores (O'Brien et al., 2013) were
74 used to explore the impact of size and key culturing parameters on the percentage of cells that
75 are diffusion limited. Biomass Zn/P ratios were assumed to be around 2 mmol mol⁻¹, the mean
76 intra-cellular value for various natural communities (Twining and Baines, 2013; Twining et al.,
77 2003) and found in previous culture experiments (Sunda and Huntsman, 1992). These Zn/P
78 ratios were converted to absolute cellular Zn quotas using previously-suggested empirical
79 relationships for calculating the carbon biomass from cell volumes (Leblanc et al., 2012;
80 Smayda, 1978; Sun and Liu, 2003) and a Redfield C/P ratio of 106/1.

81 The maximum diffusion rate (ρ) was assessed using $\rho = 4\pi rD [Me']$, where $[Me']$ represents the
82 inorganic metal concentration in the medium outside the cell. The radius (r) was derived from
83 the biovolume by assuming all cells to be spherical (Sunda and Huntsman, 1992). Values of $6 \cdot$
84 $10^{-6} \text{ cm}^2 \text{ s}^{-1}$ (Sunda and Huntsman, 1992) and $9 \cdot 10^{-6} \text{ cm}^2 \text{ s}^{-1}$ (Hudson and Morel, 1990) were
85 used for the diffusion rate constant (D) of Zn and Fe, respectively.

86 As a result of this (rather strict) assessment, Zn' was set to a value of about 0.1 nmol l⁻¹. Two
87 thirds of all the 1362 MAREDAT diatoms and 181 coccolithophores are not diffusion limited at
88 this Zn concentration, up to growth rates of 0.8 d⁻¹, and for cellular Zn/P ratios <2 mmol mol⁻¹
89 (Fig. S.1B). This Zn' concentration is above the threshold where diffusion limited uptake of Zn
90 starts to matter, for a variety of differently sized phytoplankton. Conversely, the proportion of
91 phytoplankton not limited by diffusion is higher the less Zn is taken up into the cell (Fig. S.1C),
92 or the slower the growth (Fig. S.1D), assuming the other two parameters to remain constant. In

93 this context, it is important to keep in mind that the definition applied here of where diffusion
94 limitation begins is rather strict. Underlying our definition is the assumption that the surface is
95 100% covered in Zn transporters, which is of course not possible as there must be transporters
96 of other nutrients too, as well as structural proteins, phospholipids, and other cell wall
97 components. Sunda and Huntsman (1992) thus suggest that diffusion limitation of *E. huxleyi*
98 and *T. pseudonana* might begin as early as at ~ 30% of the maximum diffusive flux (Hudson
99 and Morel, 1993). In the light of such considerations it important not to get too close to the
100 calculated concentration threshold in culture experiments that are not designed to be diffusion
101 limited.

102 This can also be examined from the perspective of cellular A/V ratios. If similar cellular Zn
103 quotas taken up into smaller *versus* larger cells, small cells (large A/V ratio) will begin to suffer
104 from diffusion limitation at lower Zn' (Fig. S.1E) compared to larger cells (small A/V ratio). It
105 is important to note that this theoretically predicted effect is typically compensated by the fact
106 that small cells grow much more slowly than larger ones, and that often they also do not take up
107 as much Zn. For *T. weissflogii*, the largest diatom studied here, Zn' concentrations as low as
108 0.01 nmol l⁻¹ would come with severe diffusion limitation (red square in Fig. S.1A). On the
109 other hand, at the chosen Zn' level of 0.1 nmol l⁻¹, cellular Zn/P ratios can be as high as 4 mmol
110 mol⁻¹ (Fig. S.1F), and growth rates as high as 1.6 d⁻¹ (Fig. S.1G), without diffusion limitation of
111 Zn uptake in *T. weissflogii*. However, it worth noting that a unimodal relationship between
112 phytoplankton growth rate and cell size has previously been described by Chen and Liu (2010),
113 when temperature and nutrient availability are accounted for.

114 **S.3 UV-VIS-NIR absorbance spectrophotometry and *in vivo* fluorescence**

115 An important aim of this contribution is to explore species dependent isotope effects associated
116 with Zn uptake into the cell, covering the diversity of cyanobacteria to the greatest possible
117 extent. In order to achieve this aim, robust criteria are needed to distinguish the different
118 strains. Large eukaryotic phytoplankton tends to offer criteria that can be used for
119 discrimination, which also help to distinguish ecologically and evolutionary distinct species.

120 For prokaryotes, by contrast visual features, detectable *e.g.* by light microscopy, are often
121 ambiguous. Instead, molecular methods such as the sequencing of nucleic acids are commonly
122 used to capture diversity among prokaryotes. To some degree, the budgets of different
123 photosynthetic pigments in cultured cells can be used. The color of dense monocultures can
124 provide a first indication of the cellular budget of photosynthetic pigments in cyanobacteria,
125 and thus the identity of the organism. The absorbance of ultraviolet (UV), visible (VIS), and
126 near-infrared (NIR) light, together with *in vivo* fluorescence in response to monochromatic
127 light, can provide further information on the photo-physiological capabilities and the molecular
128 structure of the light harvesting apparatus in living cyanobacterial cells.

129 A combination of UV-VIS-NIR and *in vivo* fluorescence (Supplementary Figure S.2) was thus
130 used to verify that all four of the cyanobacteria here are distinct in the molecular structure and
131 composition of their light harvesting complexes, namely their phycobilisomes. The molecular
132 structure of the light harvesting apparatus is not only resulting the complex evolutionary history
133 of prokaryotes, it also significantly contributes to the color of dense monocultures.
134 *Prochlorococcus marinus* and three *Synechococcus* strains (see Section 2.1) were chosen to
135 cover a range of different colors, reflecting structural differences in their photosynthetic
136 apparatus. Two of the chosen *Synechococcus* strains (CCMP 1334 and 2370; Scanlan et al.,
137 2009; Six et al., 2007; Six et al., 2005; Six et al., 2004; Toledo et al., 1999) and *P. marinus*
138 (CCMP 2389; Biller et al., 2015; Moore et al., 1995; Scanlan et al., 2009; Ting et al., 2002)
139 were previously well characterized with respect to their light harvesting architecture. Unlike
140 other green strains such as CCMP 1333 (*a.k.a.* WH 5701, see *e.g.*, Six et al., 2007), the green
141 representative of the genus *Synechococcus* (CCMP 1183) used here has not previously been
142 shown to have a phycocyanin dominated phyobiliprotein composition.

143 All spectrofluorometric *in vivo* analyses were done during exponential growth phase using an
144 Infinite[®] 200 Pro plate reader (Tecan, Switzerland). Absorbance spectra were recorded for the
145 wavelength range 350 to 750 nm, in step sizes of 1 nm (Supplementary Figure S.2). The blank
146 corrected absorbance of every species was individually normalized to the measurement with the

147 least transmittance. The excitation wavelength chosen to obtain fluorescence spectra was set to
148 the observed absorbance maxima and hence to values of 390, 415, 440, 495, 550, and 630 nm,
149 for all four cyanobacteria strains. Fluorescence readings were typically recorded from 800 nm
150 down to 30 nm above the excitation wavelength, in a step size of 2 nm, with emission
151 intensities integrated over 20 μ s. Inter-species differences in absolute intensities were preserved
152 by normalizing all fluorescence data to the maximum emission recorded among all four
153 cyanobacteria strains.

154 **S.4 Distinguishing cyanobacteria via their photosynthetic apparatus**

155 All studied phytoplankton is harvesting light with antenna complexes, called phycobilisomes,
156 which are differing in their molecular structure between different organisms. Classification of
157 all here investigated strains to groups of distinct light harvesting strategies was confirmed using
158 previously established techniques. The framework for doing this was established by Six et al.
159 (2007) for evolutionary distinct *Synechococcus* strains, which were then compared to
160 *Prochlorococcus marinus* following Moore et al. (1995), Ting et al. (2002) and Biller et al.
161 (2015).

162 *Synechococcus* cells owe their vivid colors (Fig. S.3A) to the macromolecular structure of their
163 phycobilisomes (Glazer, 1989; Glazer et al., 1985), with rods made of phycobiliproteins
164 surrounding a central allophycocyanin core (Scanlan et al., 2009; Six et al., 2007). Only in
165 some *Synechococcus* strains does phycocyanin (PC) constitute the whole rod (Type 1 according
166 to Six et al., 2007): in most cases PC only makes up the basal end of the rod while most of it is
167 phycoerythrin (Fig. S.3B; Type 2 and 3 according to Six et al., 2007). All type 3 strains,
168 however, contain the red and orange colored chromophores phycoerythrobilin (PEB, $A_{\max} =$
169 550 nm) and phycourobilin (PUB, $A_{\max} = 495$ nm) in variable proportions (Fig. S.3C),
170 according to their preferred light niche. The *Synechococcus* strain CCMP 1183 has not
171 previously been categorized into any of these types, while CCMP 1334 and 2370 are known to
172 be of type 3a and 3c, respectively (Six et al., 2007). Six et al. (2007) recommend distinguishing
173 the latter two types using fluorescence excitation maxima ($F_{495\text{ nm}} / F_{550\text{ nm}}$) emitting at around

174 580 nm, since the carotenoids zeaxanthin and β -carotene interfere with the characteristic
175 absorbance ratio ($A_{495\text{ nm}} / A_{550\text{ nm}}$). For CCMP 1334 and 2370, PUB / PEB ratios are 0.457 and
176 1.829, as obtained with white light, and are in very good agreement with previously reported
177 values of 0.440 and 1.856 (Six et al., 2007). The lack of fluorescence emitted at 580 nm ruled
178 out types 2 or 3 due to the absence of phycoerythrin in CCMP 1183, while pronounced
179 emissions at ~ 660 nm, excited at ~ 630 nm, indicate the dominance of PC instead (Type 1).

180 *Prochlorococcus marinus* (CCMP 2389) is well known be one of the few cyanobacteria strains
181 (together with *Prochloron* and *Prochlorothrix*) that lack phycobilisomes (Fig. S.3B; Biller et
182 al., 2015), but possesses a divinyl chlorophyll a and b binding protein (Biller et al., 2015;
183 Chisholm et al., 1992). Significant proportions of this pigment typically express a lime-green
184 color in dense pure *Prochlorococcus* cultures (Fig. S.3D; Lindell, 2014). This distinctive
185 pigmentation supports more efficient absorption of green light due to a blue-light absorbance
186 maximum which, in comparison to other phycoerythrin free species (e.g., CCMP 1183), is
187 shifted towards higher wavelength (Fig. S.3C).

188 **S.5 Speculations on the anomalous metal quotas and $\Delta^{66}\text{Zn}$ of CCMP 2370**

189 Cox and Saito (2013), found that relative metallothionein (MT) abundances rose when Zn was
190 added to CCMP 2370 cultures, and that this was accentuated at low PO_4^{3-} . This suggests the
191 possibility of a link to PO_4^{3-} acquisition, since alkaline phosphatases (PhoA) require Zn. High
192 cellular MT contents could thus also explain high biomass Zn/P ratios, as observed for CCMP
193 2370. Although an explanation for the exact use of MT is still elusive (Palmiter, 1998), two
194 functionalities seem likely. Firstly, MT could build up a cellular Zn reservoir, serve as a
195 chaperon to transport Zn to Zn-containing proteins, and ultimately detoxify the cell if
196 intracellular divalent metal contents get too high. Secondly, it has also been suggested as a
197 potentially very powerful antioxidant, preventing accumulation of oxygen (O) radicals (Cox
198 and Saito, 2013; Palmiter, 1998; Robinson et al., 2001). Zn in MT is four-fold coordinated via
199 thiol groups, or is arranged in more complex ZnS clusters of variable structure and
200 stoichiometry (Maret et al., 1997; Maret and Vallee, 1998). If published *ab-initio* calculations

201 of the equilibrium isotope fractionation between Zn^{2+} and the amino acid cysteine (Fujii et al.,
202 2014) are representative for such clusters, one could speculate that they would preferentially
203 bind heavy Zn isotopes. If Zn efflux from the cell derives exclusively from the non-MT-bound
204 intracellular Zn pool, this could cause enrichment of heavy Zn-isotopes in the phytoplankton
205 cell, while light Zn is continuously re-exported to the ambient medium. Dupont et al. (2008)
206 show that clone CCMP 2370 has a strong requirement for Ni in superoxide dismutase (SOD)
207 but does not have the genes for Zn or Cu SOD. The necessity to detoxify an excess of
208 intracellular Zn might thus also differentiate CCMP 2370 from the other studied strains.

209 Phycourobilin PUB has a light absorption maximum at a wavelength of around 495 nm (blue-
210 green). In coastal settings, where scattering by particles significantly reduces light penetration
211 depth, this is the part of the light spectrum that reaches deepest into the water column (Wozniak
212 and Dera, 2007). One could speculate that CCMP 2370 is possibly better adapted to deeper
213 open ocean or coastal ecological niches compared to the other *Synechococcus* strains (not
214 *Prochlorococcus*). Such environments, both deep open marine and coastal, are often Zn-rich in
215 comparison to the shallowest open ocean. A metabolism that is evolutionarily adapted to such
216 an environment would not necessarily need to economize its Zn use. It is perhaps noteworthy,
217 then, that *P. marinus* is perhaps one of the best documented examples of a cyanobacterium that
218 persists deeper in the water column. The high-light adapted strain used for experimentation
219 here, however, originates from a water depth of only 5 m in the Mediterranean and might not be
220 representative of depth-adapted *Prochlorococcus* cells.

221 An alternative irradiance-based scenario to explain unusually high Zn quotas associated with
222 CCMP 2370 could be that the irradiance levels used in culture are the farthest away from the
223 natural habitat of this strain. Finkel et al. (2006) consistently observe higher cellular Zn and Fe
224 quotas among various light limited phytoplankton, but this seems unlikely to explain the data
225 for CCMP 2370 as its type 3c photosynthetic apparatus should still allow it to capture blue-
226 green light when other phototrophs might become growth limited. The culture experiment here
227 was done with white light. Given that CCMP 2370 might be adapted to a blue-green niche, it

228 seems imaginable that inappropriate light-spectra might cause similar effects. Currently, it can
229 only be speculated about possible mechanisms, but the need to detoxify the cell of unwanted
230 photosynthetic by-products, such as oxygen radicals, by means of Zn-containing proteins (Cox
231 and Saito, 2013; Palmiter, 1998) could be one way to explain the higher cellular Zn budget.

232 **S.6 Fe and Zn use efficiencies of pro- versus eukaryotes**

233 Sunda and Huntsman (2015) further developed a scheme, first established by Raven (1990),
234 that allows computing how much atmospheric CO₂ is fixed into marine biomass per Fe atom.
235 The coastal diatom *Thalassiosira pseudonana* was previously found to build up more biomass
236 per Fe atom than the cyanobacterium *Synechococcus bacillaris* (Sunda and Huntsman, 2015).
237 In other words, eukaryotic diatoms tend to use Fe more efficiently than prokaryotic
238 cyanobacteria. Analogous to this approach, we calculate the iron use efficiency (IUE) by
239 dividing the specific growth rate of an organism by its cellular Fe/P ratio. The interest in
240 comparing IUEs among different phytoplankton originates with the hypothesis that modern
241 prokaryotes require higher cellular Fe contents, as a vestige from the time when they first
242 evolved in a primordial ocean rich in Fe, later than eukaryotes.

243 In contrast to Fe, the Precambrian ocean is assumed to be lower in its Zn inventory than the
244 modern (Anbar, 2008; Zerkle et al., 2005), posing the question of whether the cellular Zn
245 content of phytoplankton would then also need to be the reverse of Fe (Saito et al., 2003). Our
246 cellular Fe and Zn quotas seem to support both hypotheses (Fig. 3A and B), with the caveat that
247 one cyanobacterial strain records the highest measured Zn/P ratio in the entire dataset (CCMP
248 2370, *c.f.* Section 4.1 and 4.2). IUEs provide an important advantage over absolute cellular
249 quotas in that they consider specific growth rates in their calculation routine. If growth is
250 suppressed in culture because laboratory conditions differ from the natural habitat, which is
251 supposedly the case for CCMP 2370, this is partly accounted for by IUEs. It is only ‘partly’
252 accounted for, as the cell might still have needed to adapt its metallo-proteome to achieve the
253 observed growth rate. But, without proteomic data, usage efficiencies might be as close as one
254 currently can get to quantifying species-dependent differences independent of environmental

255 factors. Here, we thus take this concept further and extend it to zinc use efficiencies (ZUE),
256 which we use to further explore the dependency of both metal usage efficiencies on the cellular
257 metal quota and those of the other element, respectively.

258 Both IUE and ZUE decrease with increasing cellular Fe and Zn quotas (Fig. S.4A and B). The
259 highest Zn use efficiencies were observed in representatives of the prokaryotic genus
260 *Synechococcus* with Fe/P ratios in the range between ~4 and 5.5 mmol mol⁻¹ (Fig. S.4C). The
261 biomass elements C and P, in contrast, are most efficiently built up per Zn atom in eukaryotic
262 marine diatoms with cellular Zn/P ratios of ~1.5 to 2 mmol mol⁻¹ (Fig. S.4D). This behavior is
263 in strong contrast to what can be observed for Fe and Zn uptake rates (Fig. S.4E and F), where
264 diatoms consistently transport most metals per surface area and unit time. It is an intriguing –
265 though unexplained – observation that the most efficient metal usage coincides almost exactly
266 with the numbers that previously reported as the global average of intracellular Fe and Zn
267 quotas of phytoplankton (Fig. S.4C and D), as obtained from synchrotron-based X-ray
268 fluorescence imaging techniques (*e.g.*, Twining and Baines, 2013).

269 Based on the coupling of Zn and Fe uptake rates in an Fe-limitation scenario both metals were
270 previously speculated to be physiologically linked to each other in marine diatoms (Köbberich
271 and Vance, 2017). The metal use efficiencies explored here might shed further light on this
272 idea. It might thus not be coincident that ZUEs are highest around the global average of
273 intracellular Fe/P ratios (Fig. S.4C), while IUEs peak around the global average of intracellular
274 Zn/P (Fig. S.4D). This raises the question as to whether global average cellular quotas are the
275 natural consequence of a potentially rather narrow physiological window that allows the most
276 efficient build-up of bio-elements. Consistent with the hypothesis that modern prokaryotes
277 require higher cellular Fe contents than later evolved eukaryotes, all diatoms studied here were
278 consistently found to use Fe more efficiently than most cyanobacteria, except CCMP 2370 (Fig.
279 S.4D).

280 It is, however, important to note that metal use efficiencies, as calculated by dividing the
281 growth rate by a cellular quota, are minimum estimates. Proper characterization of these values

282 requires growth under nutrient limitation. The set of experiments presented here was performed
283 at a single pair of Fe and Zn concentrations, so it cannot conclusively be determined whether a
284 strain uses Zn inefficiently, or if cells use Zn at high efficiency but with a large amount of Zn
285 storage. One might infer from Table 1 that *Prochlorococcus* has a lower Zn use efficiency, but
286 there is no evidence that *Prochlorococcus* requires Zn to grow, meaning it could have an
287 infinitely high Zn use efficiency (Saito & Moffett, 2001).

288 **References**

- 289 Anderson, M.A., Morel, F.M.M., Guillard, R.R.L., 1978. Growth limitation of a coastal diatom
290 by low zinc ion activity. *Nature*, 276: 70-71.
- 291
- 292 Berges, J.A., Franklin, D.J., Harrison, P.J., 2001. Evolution of an artificial seawater medium:
293 improvements in enriched seawater, artificial water over the last two decades. *Journal*
294 *of Phycology*, 37: 1138-1145.
- 295
- 296 Biller, S.J., Berube, P.M., Lindell, D., Chisholm, S.W., 2015. *Prochlorococcus*: the structure
297 and function of collective diversity. *Nature Reviews Microbiology*, 13: 13-27.
- 298
- 299 Chen, B., Liu, H., 2010. Relationships between phytoplankton growth and cell size in surface
300 oceans: Interactive effects of temperature, nutrients, and grazing. *Limnology and*
301 *Oceanography*, 55: 965-972.
- 302
- 303 Chisholm, S., 1992. Phytoplankton Size. In: Falkowski, P., Woodhead, A., Vivirito, K. (Eds.),
304 Primary Productivity and Biogeochemical Cycles in the Sea. Environmental Science
305 Research. Springer, pp. 213-237.
- 306
- 307 Cox, A.D., Saito, M.A., 2013. Proteomic responses of oceanic *Synechococcus* WH8102 to
308 phosphate and zinc scarcity and cadmium additions. *Frontiers in Microbiology*, 4: 387,
309 pp. 1-17.
- 310
- 311 Dupont, C.L., Barbeau, K., Palenik, B., 2008. Ni uptake and limitation in marine
312 *Synechococcus* strains. *Applied and environmental microbiology*, 74: 23-31.
- 313
- 314 Finkel, Z.V. et al., 2006. Irradiance and the elemental stoichiometry of marine phytoplankton.
315 *Limnology and Oceanography*, 51: 2690-2701.
- 316
- 317 Fujii, T., Moynier, F., Blichert-Toft, J., Albarède, F., 2014. Density functional theory
318 estimation of isotope fractionation of Fe, Ni, Cu, and Zn among species relevant to
319 geochemical and biological environments. *Geochimica et Cosmochimica Acta*, 140:
320 553-576.
- 321
- 322 Glazer, A.N., 1989. Light guides. Directional energy transfer in a photosynthetic antenna.
323 *Journal of Biological Chemistry*, 264: 1-4.
- 324
- 325 Glazer, A.N., Chan, C., Williams, R.C., Yeh, S.W., Clark, J.H., 1985. Kinetics of Energy Flow
326 in the Phycobilisome Core. *Science*, 230: 1051-1053.
- 327
- 328 Harrison, P.J., Thompson, P.A., Calderwood, G.S., 1990. Effects of nutrient and light limitation
329 on the biochemical composition of phytoplankton. *Journal of Applied Phycology*, 2:
330 45-56.
- 331

332 Hudson, R.J.M., Morel, F.M.M., 1990. Iron transport in marine phytoplankton: kinetics of
333 cellular and medium coordination reactions. *Limnology and Oceanography*, 35: 1002-
334 1020.

335

336 Hudson, R.J.M., Morel, F.M.M., 1993. Trace metal transport by marine microorganisms:
337 implications of metal coordination kinetics. *Deep Sea Research*, 20: 129-150.

338

339 John, S.G., Geis, R.W., Saito, M.A., Boyle, E.A., 2007. Zinc isotope fractionation during high-
340 affinity and low-affinity zinc transport by the marine diatom *Thalassiosira oceanica*.
341 *Limnology and Oceanography*, 52: 2710-2714.

342

343 Köbberich, M., Vance, D., 2017. Kinetic control on Zn isotope signatures recorded in marine
344 diatoms. *Geochimica et Cosmochimica Acta*, 210: 97-113.

345

346 Laloui, W. et al., 2002. Genotyping of axenic and non-axenic isolates of the genus
347 *Prochlorococcus* and the OMF-‘*Synechococcus*’ clade by size, sequence analysis or
348 RFLP of the Internal Transcribed Spacer of the ribosomal operon. *Microbiology*, 148:
349 453-465.

350

351 Leblanc, K. et al., 2012. A global diatom database – abundance, biovolume and biomass in the
352 world ocean. *Earth System Science Data*, 4: 149-165.

353

354 Lindell, D., 2014. The Genus *Prochlorococcus*, Phylum Cyanobacteria. In: Rosenberg, E.,
355 DeLong, E., Lory, S., Stackebrandt, E., Thompson, F. (Eds.), *The Prokaryotes*.
356 Springer Berlin Heidelberg, pp. 829-845.

357

358 Maret, W., Larsen, K.S., Vallee, B.L., 1997. Coordination dynamics of biological zinc
359 “clusters” in metallothioneins and in the DNA-binding domain of the
360 transcription factor Gal4. *Proceedings of the National Academy of Sciences*, 94: 2233-
361 2237.

362

363 Maret, W., Vallee, B.L., 1998. Thiolate ligands in metallothionein confer redox activity on zinc
364 clusters. *Proceedings of the National Academy of Sciences*, 95: 3478-3482.

365

366

367 Moore, L.R., Goericke, R., Chisholm, S.W., 1995. Comparative physiology of *Synechococcus*
368 and *Prochlorococcus*: influence of light and temperature on growth, pigments,
369 fluorescence and absorptive properties. *Marine Ecology Progress Series*, 116: 259-275.

370

371 Moore, L.R., Rocap, G., Chisholm, S.W., 1998. Physiology and molecular phylogeny of
372 coexisting *Prochlorococcus* ecotypes. *Nature*, 393: 464-7.

373

374 Moore, L.R., Chisholm, S.W., 1999. Photophysiology of the marine cyanobacterium
375 *Prochlorococcus*: Ecotypic differences among cultured isolates, *Limnology and*
376 *Oceanography*, 44, 628–638.

377

378 Moore, L.R., Post, A.F., Rocap, G., Chisholm, S.W., 2002. Utilization of different nitrogen
379 sources by the marine cyanobacteria *Prochlorococcus* and *Synechococcus*. *Limnology and*
380 *Oceanography*, 47: 989–996.

381
382 Moore, L.R. et al., 2007. Culturing the marine cyanobacterium *Prochlorococcus*. *Limnology and*
383 *Oceanography: Methods*, 5: 353-362.

384
385 Morel, F.M.M., Rueter, J.G., Anderson, D.M., Guillard, R.R.L., 1979. AQUIL: a chemically
386 defined phytoplankton culture medium for trace metal studies. *Journal of Phycology*,
387 15: 135-141.

388
389 O'Brien, C.J. et al., 2013. Global marine plankton functional type biomass distributions:
390 coccolithophores. *Earth System Science Data*, 5: 259-276.

391
392 Palmer, R.D., 1998. The elusive function of metallothioneins. *Proceedings of the National*
393 *Academy of Sciences*, 95: 8428-8430.

394
395
396 Price, N.M. et al., 1989. Preparation and chemistry of the artificial algal culture medium Aquil.
397 *Biological Oceanography*, 6: 443-461.

398
399 Raven, J.A., 1990. Predictions of Mn and Fe use efficiencies of phototrophic growth as a
400 function of light availability for growth and of C assimilation pathway. *New*
401 *Phytologist*, 116: 1-18.

402
403 Rippka, R. et al., 2000. *Prochlorococcus marinus* Chisholm et al. 1992 subsp. *pastoris* subsp.
404 nov. strain PCC 9511, the first axenic chlorophyll a2/b2-containing cyanobacterium
405 (Oxyphotobacteria). *International Journal of Systematic and Evolutionary*
406 *Microbiology*, 50: 1833-1847.

407
408 Robinson, N.J., Whitehall, S.K., Cavet, J.S., 2001. Microbial metallothioneins, *Advances in*
409 *Microbial Physiology*. Academic Press, pp. 183-213.

410
411 Rodushkin, I., Stenberg, A., Andrén, H., Malinovsky, D., Baxter, D.C., 2004. Isotopic
412 fractionation during diffusion of transition metal ions in solution. *Analytical*
413 *Chemistry*, 76: 2148-2151.

414
415 Saito, M.A., Moffett, J.W., 2001. Complexation of cobalt by natural organic ligands in the
416 Sargasso Sea as determined by a new high-sensitivity electrochemical cobalt speciation
417 method suitable for open ocean work. *Marine chemistry*, 75: 49-68.

418
419 Saito, M.A., Sigman, D.M., Morel, F.M.M., 2003. The bioinorganic chemistry of the ancient
420 ocean: the co-evolution of cyanobacterial metal requirements and biogeochemical
421 cycles at the Archean–Proterozoic boundary? *Inorganica Chimica Acta*, 356: 308-318.

422

- 423 Samanta, M., Ellwood, M.J., Strzepek, R.F., 2017. Zinc isotope fractionation by *Emiliania*
424 *huxleyi* cultured across a range of free zinc ion concentrations. *Limnology and*
425 *Oceanography*: 63: 660-671.
- 426
- 427 Scanlan, D.J. et al., 2009. Ecological Genomics of Marine Picocyanobacteria. *Microbiology*
428 *and Molecular Biology Reviews*, 73: 249-299.
- 429
- 430 Six, C. et al., 2007. Diversity and evolution of phycobilisomes in marine *Synechococcus* spp.: a
431 comparative genomics study. *Genome Biology*, 8: R259.
- 432
- 433 Six, C. et al., 2005. Two Novel Phycoerythrin-Associated Linker Proteins in the Marine
434 Cyanobacterium *Synechococcus* sp. Strain WH8102. *Journal of Bacteriology*, 187:
435 1685-1694.
- 436
- 437 Six, C., Thomas, J.C., Brahamsha, B., Lemoine, Y., Partensky, F., 2004. Photophysiology of
438 the marine cyanobacterium *Synechococcus* sp. WH8102, a new model organism.
439 *Aquatic Microbial Ecology* 35: 17-29.
- 440
- 441 Smayda, T.J., 1978. From phytoplankters to biomass. In: Sournia, A. (Ed.), *Phytoplankton*
442 *manual*. Museum National d'Histoire Naturelle, Paris, pp. 273-279.
- 443
- 444 Sun, J., Liu, D., 2003. Geometric models for calculating cell biovolume and surface area for
445 phytoplankton. *Journal of Plankton Research*, 25: 1331-1346.
- 446
- 447 Sunda, W.G., Huntsman, S.A., 1992. Feedback interactions between zinc and phytoplankton in
448 seawater. *Limnology and Oceanography*, 37: 25-40.
- 449
- 450 Sunda, W., Huntsman, S., 2015. High iron requirement for growth, photosynthesis, and low-
451 light acclimation in the coastal cyanobacterium *Synechococcus bacillaris*. *Frontiers in*
452 *Microbiology*, 6: 561.
- 453
- 454 Sunda, W.G., Price, N.M., Morel, F.M.M., 2005. Trace metal ion buffers and their use in
455 culture studies. In: Andersen, R.A. (Ed.), *Algal Culturing Techniques*. Academic Press,
456 Burlington.
- 457
- 458 Ting, C.S., Rocap, G., King, J., Chisholm, S.W., 2002. Cyanobacterial photosynthesis in the
459 oceans: the origins and significance of divergent light-harvesting strategies. *Trends in*
460 *Microbiology*, 10: 134-142.
- 461
- 462 Toledo, G., Palenik, B., Brahamsha, B., 1999. Swimming Marine *Synechococcus* Strains with
463 Widely Different Photosynthetic Pigment Ratios Form a Monophyletic Group. *Applied*
464 *and Environmental Microbiology*, 65: 5247-5251.
- 465

- 466 Twining, B.S. et al., 2003. Quantifying trace elements in individual aquatic protist cells with a
467 synchrotron X-ray fluorescence microprobe. *Analytical Chemistry*, 75: 3806-3816.
- 468
- 469 Twining, B.S., Baines, S.B., 2013. The trace metal composition of marine phytoplankton.
470 *Annual Review of Marine Science*, 5: 191-215.
- 471
- 472 Wozniak, B., Dera, J., 2007. *Light Absorption in Sea Water*. Atmospheric and oceanographic
473 sciences library. Springer.
- 474
- 475 Zerkle, A.L., House, C.H., Brantley, S.L., 2005. Biogeochemical signatures through time as
476 inferred from whole microbial genomes. *American Journal of Science*, 305: 467-502.

477 **Figure captions**

478 *two-column fitting image: Fig. S.1.* The MARine Ecosystem DATa (MAREDAT; Buitenhuis et
479 al., 2013) was used to find culturing conditions that avoid diffusion limitation despite variably-
480 sized phytoplankton cells. The ratio of the Zn uptake rate over the maximum diffusion rate
481 represents a measure of where growth starts to become diffusion limited, which is strongly
482 dependent on the bioavailable Zn concentration (A). The percentage of the entire dataset that is
483 not diffusion limited (solid line) for variable growth conditions (B-D), with the dashed line
484 marking 2/3 of the total. Panels E-G investigate the boundary between diffusion-limitation
485 (which occurs below the solid lines in all three panels) and its absence as a function of the ratio
486 of surface area to biovolume (A/V). Even the largest diatom cultured here (horizontal dashed
487 line) has an A/V ratio that lies in the non-diffusion-limited field for the chosen bioavailable Zn
488 concentration (vertical red line in E) and would remain there for Zn/P ratios as high as 4 mmol
489 mol⁻¹, or growth rates as high as 1.6 d⁻¹.

490 *full page: Fig. S.2.* Absorbance and fluorescence spectra of all four measured cyanobacteria
491 strains. From left to right: *Prochlorococcus marinus* (CCMP 2389), and the three
492 *Synechococcus sp.* CCMP 1183, CCMP 1334, and CCMP 2370.

493 *single-column fitting image: Fig. S.3.* Illustration of how cyanobacteria owe their vivid colors
494 to the interplay between the absorbance spectra of photosynthetic pigments and the
495 macromolecular structure of their light harvesting apparatus (phycobilisome).

496 *two-column fitting image: Fig. S.4.* The relationships between Fe and Zn use efficiencies and
497 cellular metal quotas (A and B), their relationship to the quota of the other element (C and D),
498 and a comparison between surface area normalized Zn uptake rates and element quotas relative
499 to P (E and F). The dashed line is showing the global average Fe/P and Zn/P in oceanic
500 phytoplankton from Twining and Baines (2013).

1 1 **Zn isotope fractionation during uptake into**
2
3
4 2 **marine phytoplankton: implications for**
5
6
7 3 **oceanic zinc isotopes**
8
9

10
11
12
13
14 4 **Michael Köbberich^{1*} and Derek Vance¹**
15
16

17
18 5 *To whom correspondence should be addressed
19
20
21
22

23
24
25 6 Submitted to: *Chemical Geology*

26
27 7 Special issue: *GEOTRACES - Goldschmidt Session 10i*
28
29
30
31

32
33
34 8
35
36
37 9 **Corresponding author**

38 10 Michael Köbberich, phone: +41 (0) 44 632 07 30, email: michael.koebberich@alumni.ethz.ch
39
40

41 11 **Author affiliations**

42 12 ¹ Institute of Geochemistry and Petrology, Department of Earth Sciences, ETH Zurich,
43 13 Clausiusstrasse 25, CH-8092 Zurich, Switzerland
44
45
46

47 14 **Running head**

48 15 Ligand controlled Zn isotope fractionation
49
50
51

52 16 **Keywords**

53 17 Zinc isotopes, Ligands, Phytoplankton culturing, Metal uptake, GEOTRACES, Trace Metals.
54
55
56
57
58
59
60
61
62
63
64
65

18 **Abstract**

19 The extreme scarcity of zinc (Zn) in the euphotic zone, coupled to deep enrichments, is
20 consistent with biological uptake at the surface and regeneration at depth. In the context of a
21 nutrient-type depth profile so clearly shaped by uptake into phytoplankton, the growing dataset
22 for Zn isotopes presents a challenge. These data either show very minor isotope effects
23 associated with extreme depletion, or enrichment of the light isotopes in the upper ocean. In
24 contrast, culturing of eukaryotes in the laboratory suggests that light Zn isotopes are
25 preferentially taken up into diatoms and coccoliths, implying that Zn depletion at the surface
26 should be associated with extremely heavy residual dissolved signals.

27 Here we present the first Zn isotope measurements for cultured marine cyanobacteria and
28 compare these data to those for eukaryotic diatoms grown under identical conditions. Of the
29 four cyanobacteria cultured, belonging to the genera *Synechococcus* and *Prochlorococcus*,
30 three preferentially take up light Zn into the cell, with a variability that is not fundamentally
31 different between pro- and eukaryotic phytoplankton. We also observe only very subtle
32 differences between Zn/P and Fe/P uptake ratios for these three cyanobacteria groups relative to
33 diatoms grown under the same conditions. A fourth strain exhibits preferential uptake of heavy
34 Zn isotopes, and very high Zn/P ratios. Overall, we speculate that the observed variability
35 among cyanobacteria may be related to the molecular structure of their photosynthetic light
36 harvesting apparatus, adapted to significantly different light niches.

37 These new and published culture data support the hypothesis that cellular $\delta^{66}\text{Zn}$ in culture
38 might largely be controlled by the organic ligands that bind Zn in the medium. Given that the
39 Zn-binding ligands in the ocean have thermodynamic stability constants that are orders of
40 magnitude smaller than the EDTA used in culture media, the surprisingly subtle Zn isotope
41 variability in some parts of the surface ocean may be reconciled with culture data by the lesser,
42 near zero, preference of these weaker complexes for heavy Zn isotopes.

43

44 1. Introduction

45 Intracellular metal quotas (Twining and Baines, 2013; Twining et al., 2003) show that zinc (Zn)
46 and iron (Fe) are the two most abundant trace metals in marine phytoplankton (Morel et al.,
47 2014; Twining and Baines, 2013). Extremely low bioavailable Fe concentrations limit the
48 fixation of atmospheric carbon dioxide (CO₂) by phytoplankton in about 30% of the global
49 surface ocean (Moore et al., 2013), and likely also near the deep chlorophyll maximum of
50 stratified subtropical mid-ocean gyres (Hopkinson and Barbeau, 2008; Sedwick et al., 2005;
51 Sunda and Huntsman, 2015). Although the jury is still out on whether Zn co-limits
52 phytoplankton growth in certain regions of the global ocean (*c.f.* Moore et al., 2013), Zn is
53 often equally, if not more, abundant in the cell than Fe (Twining and Baines, 2013). Both
54 metals serve as co-factors in enzymes of key metabolic pathways. Important examples of Zn
55 containing enzymes are carbonic anhydrases, essential during biomass buildup from reduced
56 carbon (C) and light (Domsic et al., 2008; Morel et al., 2014; Roberts et al., 1997), or alkaline
57 phosphatases for the acquisition of organic phosphorus (P) when phosphate is scarce (Cox and
58 Saito, 2013; Morel et al., 2014; Shaked et al., 2006). Superoxide dismutases can also require
59 sizeable fractions of the cellular Fe and Zn pool, in particular in phototrophs, where light-
60 induced reactions often come with toxic superoxide anions (O₂⁻) that can be reduced by this
61 enzyme (Morel, 2008; Wolfe-Simon et al., 2005). As a result, Zn is extremely scarce in the
62 surface ocean, while the deep ocean is enriched, consistent with biological uptake in the
63 euphotic zone and its regeneration at depth (Bruland, 1980; Bruland et al., 2014).

64 Metal stable isotope data, increasingly available through the international GEOTRACES
65 program, provide a new way of investigating the impact of trace metal availability on
66 phytoplankton growth. However, the data available to date for oceanic Zn isotopes have
67 presented some challenging puzzles. For example, despite drawdown by diatom uptake during
68 northward flow of surface waters, of close to 99% of the Zn upwelled in the Southern Ocean,
69 the Zn-depleted residual water is not shifted to very heavy values (Wang et al., this volume;
70 Zhao et al., 2014), as would be expected for preferential uptake of light isotopes into cells.

1
2
3
4
5
6
7
8
9
10
11
12
13
14
15
16
17
18
19
20
21
22
23
24
25
26
71 Furthermore, for nearly all regions outside the Southern Ocean (Conway and John, 2014;
72 Conway and John, 2015; John et al., 2018), dissolved Zn in the upper ocean is significantly
73 enriched in light Zn isotopes compared to the globally rather homogeneous deep ocean. Though
74 Samanta et al. (2017) invoke the uptake of light isotopes with decreased Zn abundances in the
75 surface Tasman Sea, the data are noisy, the correlation is very weak ($r^2 = 0.21$, MSWD = 15)
76 and the fractionation factor implied is within uncertainty of zero. The same very weak
77 relationship and near zero fractionation are seen in the data of Wang et al. (this volume). These
78 findings seem to be at odds with the expectation that light isotopes would be preferentially
79 taken up into cells, and with laboratory culture experiments that find the biomass of marine
80 eukaryotic algae to be enriched in light Zn isotopes with respect to the experimental medium
81 (John and Conway, 2014; John et al., 2007; Köbberich and Vance, 2017; Köbberich and Vance,
82 2018; Samanta et al., 2017).

27
28
29
30
31
32
33
34
35
36
37
38
39
40
41
42
43
44
45
46
47
48
49
50
51
83 Taxonomic differences among distinct groups of phytoplankton have been considered to drive
84 some of the observed regional and global variability in Zn abundances in the ocean. For
85 example, elevated Zn in diatoms (Twining and Baines, 2013) has been suggested to control
86 Southern Ocean concentrations and, through the water masses advected from it, the pattern of
87 variability in the global ocean (Vance et al., 2017). On the other hand, it is well-established that
88 cellular Zn is closely related to its bioavailability in seawater (Sunda and Huntsman, 1992),
89 leaving it unclear to what extent changes in the proteome are relevant (Cox and Saito, 2013;
90 Twining and Baines, 2013). Beyond diatoms, Samanta et al. (2017) observed electron transport
91 rates and the photosynthetic efficiency to increase with increasing free Zn^{2+} concentration in
92 another eukaryote, *Emiliana huxleyi*, which was speculated to be due to increased carbonic
93 anhydrase activity.

52
53
54
55
56
57
58
59
60
61
62
63
64
65
94 The global biogeography of phytoplankton is such that a great deal of the total chlorophyll
95 belongs to only two major groups of phytoplankton, namely *Synechococcus* or
96 *Prochlorococcus* (Follows and Dutkiewicz, 2010; Follows et al., 2007; Menemenlis et al.,
97 2005). Furthermore, these prokaryotic cyanobacteria are direct descendants of the earliest

1
2
3
4
5
6
7
8
9
10
11
12
13
14
15
16
17
18
19
20
21
22
23
24
25
26
27
28
29
30
31
32
33
34
35
36
37
38
39
40
41
42
43
44
45
46
47
48
49
50
51
52
53
54
55
56
57
58
59
60
61
62
63
64
65

98 oxygenic phototrophs, originating during a period of Earth history distinctly different in its
99 ocean chemistry (Falkowski and Knoll, 2007; Knoll et al., 2012; Saito et al., 2003; Sunda and
100 Huntsman, 2015). It has been suggested that this resulted in elevated minimum Fe requirements
101 in prokaryotes, and that this explains their high requirement for Fe relative to eukaryotes in the
102 modern ocean (Brand, 1991; Österberg, 1974; Saito et al., 2003; Sunda and Huntsman, 2015).

103 In the light of these considerations, constraints on how cyanobacteria take up Zn and its
104 isotopes are required. Here we address this requirement. We also present new data for diatoms,
105 cultured under conditions that are as close as possible to those for the cyanobacteria. Our aim is
106 to explore the relative importance of species-dependent differences versus environmental
107 controls for trace metal systematics versus, with implications for the evolution of trace metal
108 requirements in an ocean in which the biology and chemistry have both changed through time.
109 Finally, we consider the emerging dataset for oceanic Zn isotopes in the context of these new
110 constraints, as well as published data, from culture experiments.

111

112 **2. Materials & Methods**

113 Culturing media were prepared either from salts that were of trace metal purity, or from
114 solutions that were cleaned using a chelating resin (Chelex[®] 100, Bio-Rad, USA). All ultrapure
115 water came from a Milli-Q[®] integral water purification system (Merck, Millipore, Germany)
116 with a conductivity of 18.2 MΩ·cm. Reagent grade acids used for preparative purposes were
117 twice purified by sub-boiling distillation before use (DST-1000, Savillex, USA). Handling of
118 all samples and reagents was carried out under “Class 100” clean laboratory conditions at
119 constant humidity of around 10 %, and a temperature of 21.2 ± 0.2 °C.

120 **2.1 Phytoplankton strains**

121 Three different diatoms and four distinct cyanobacteria strains, all axenic, were obtained from
122 the National Center for Marine Algae and Microbiota (NCMA), formerly known as Provasoli-
123 Guillard Center for Culture of Marine Phytoplankton (CCMP), Bigelow Laboratories, USA.

1
2
3
4
5
6
7
8
9
10
11
12
13
14
15
16
17
18
19
20
21
22
23
24
25
26
27
28
29
30
31
32
33
34
35
36
37
38
39
40
41
42
43
44
45
46
47
48
49
50
51
52
53
54
55
56
57
58
59
60
61
62
63
64
65

124 Two of the chosen diatoms, *Chaetoceros sp.* (CCMP 199) and *Thalassiosira oceanica* (CCMP
125 1005), originate from oligotrophic surface waters of the Sargasso Sea, North Atlantic. The
126 third, *Thalassiosira weissflogii* (CCMP 1336) came from coastal waters of Long Island Sound,
127 North Atlantic, USA. Three representatives of the genus *Synechococcus* (CCMP 1183, 1334,
128 and 2370, the latter two are also known as WH 7803 and 8102) and *Prochlorococcus marinus*
129 (CCMP 2389, *a.k.a.* MED 4) were chosen to represent the prokaryotic phylum of
130 cyanobacteria. All four prokaryotes are open ocean strains, two of which (CCMP 1334 and
131 2370) originate in the oligotrophic surface waters of the Sargasso Sea, North Atlantic. Sterile
132 techniques were used whenever cultures or media solutions were handled. Axenic conditions
133 were monitored by inspecting small aliquots of stained culture solutions by microscopic
134 methods.

135 An important aim of this contribution is to explore inter-species Zn isotope effects associated
136 with Zn uptake into the cell. Biological fractionation of Zn isotopes during uptake has been
137 related to active transport across the cell membrane (John et al., 2007), a mechanism that for Fe
138 has been shown to be a surface-area related process (Sunda and Huntsman, 1995; Sunda and
139 Huntsman, 1997). The set of species chosen here span the entire size range of pico- and nano-
140 phytoplankton and differ in their surface area to biovolume (A/V) ratio as calculated from their
141 cellular geometry (Fig. 1). The cellular dimensions and geometries of 1362 diatoms (Leblanc et
142 al., 2012) and 181 coccolithophores (O'Brien et al., 2013) came from the MARine Ecosystem
143 DATA (MAREDAT; Buitenhuis et al., 2013) project. Geometric models that are used for
144 calculating cell surface areas and biovolumes (Leblanc et al., 2012; Sun and Liu, 2003) can also
145 be linked to empirical carbon (C) biomass estimates (Leblanc et al., 2012; Smayda, 1978). We
146 use this information to compare our laboratory cultures with the A/V ratios that have previously
147 been considered relevant to natural environments (Fig. 1).

148 **2.2 Culturing techniques**

149 The culturing conditions were similar to Köbberich and Vance (2017). A short summary is
150 given below with the most important differences highlighted. Light was supplied to all

151 phytoplankton cultures in 15- to 9-hour day to night cycles. A constant photon flux density of
152 50 rather than 40 $\mu\text{mol m}^{-2} \text{s}^{-1}$ was used, with one important exception: the high light adapted
153 *Prochlorococcus* strain CCMP 2389 was maintained at 25 $\mu\text{mol m}^{-2} \text{s}^{-1}$, as verified with a
154 newly calibrated spherical quantum sensor LI-193 (LI-COR[®], Nebraska, USA). Cell numbers
155 for calculating specific growth rates were obtained by Coulter counting on a daily basis or by
156 using a hemocytometer, as described in Köbberich and Vance (2017).

157 The artificial culture medium, used here to allow comparison across a range of different
158 eukaryotic and prokaryotic phytoplankton organisms at similar bioavailable Zn^{2+} levels, is
159 similar to that previously reported in Köbberich and Vance (2017). This medium has a seawater
160 base adjusted to a final salinity of about 36 g kg^{-1} . Total ethylenediaminetetraacetic acid
161 (EDTA) concentrations were in the range 95 - 97 $\mu\text{mol l}^{-1}$, and Zn was kept constant to allow
162 inter-species comparison at identical bioavailable Zn. Total Zn concentrations were thus
163 adjusted to obtain free divalent Zn^{2+} and inorganically bound Zn (Zn') levels in the range 67 -
164 72 and 100 - 109 pmol l^{-1} , respectively, for all eukaryotes and *Synechococcus* strains. Aqueous
165 Zn speciation has been calculated following the recommendations of Sunda et al. (2005) and
166 references therein. The artificial seawater medium used to culture the *Prochlorococcus* strain
167 CCMP 2389 had to differ from that used for all other strains for two distinct, though related,
168 reasons. Firstly, *P. marinus* simply does not grow in the above-described broad-spectrum
169 medium. Secondly, to our knowledge, there is currently no recipe available that maintains
170 *Prochlorococcus* as well as all the other species of interest. We thus designed a newly
171 developed medium that mimics the above-described solution as closely as possible, while still
172 achieving sufficient *Prochlorococcus* growth (see Supplementary Information S.1 for further
173 details).

174 All phytoplankton cells were harvested, *i.e.* separated from their residual culturing medium, at
175 or shortly after mid exponential growth, with 0.2 μm filters, using pre-cleaned vertical twin
176 membrane centrifugal concentrators (Vivaspin 20, Sartorius, Germany). Shortly after
177 harvesting, residual media remnants were removed by washing the collected cells with UV-

178 treated equatorial Atlantic seawater, with notably low Zn in the range of 0.01 - 0.05 nmol kg⁻¹
179 (Zhao, 2011). The biomass collected on the filter was re-suspended in pre-cleaned NaCl of
180 seawater osmolality, before the resulting cell suspension was pipetted out of the centrifugal
181 concentrator. After evaporation to dryness, all samples were digested in double distilled 65%
182 HNO₃ at 120 °C for ~16 hours. After a final dry-down, all digested samples were re-dissolved
183 in 2 % HNO₃ for elemental analysis, followed by column chromatography and Zn isotopic
184 analysis (see next section).

185 **2.3 Elemental and stable isotope analysis**

186 The procedures used for elemental and stable isotope analysis are identical to those previously
187 described in Köbberich and Vance (2017) and very similar to those in previous publications
188 from this laboratory (*e.g.*, Little et al., 2016; Vance et al., 2016a; Vance et al., 2016b). In brief,
189 elemental analyses were done on a ThermoScientific Element XRTM inductively-coupled
190 plasma mass spectrometer (ICP-MS). All samples for isotope analysis were purified by anion
191 exchange chromatography (Archer and Vance, 2004; Bermin et al., 2006; Maréchal et al.,
192 1999) and were measured on a Neptune PlusTM multiple-collector inductively-coupled plasma
193 mass spectrometer (MC-ICP-MS) of the same manufacturer. Instrumental mass fractionation,
194 or that occurring during ion exchange chromatography, was corrected using the double spike
195 approach as described by Bermin et al. (2006) and Zhao et al. (2014), in combination with a
196 data reduction scheme presented by Siebert et al. (2001). Procedural blanks were estimated by
197 isotope dilution analysis and are negligible.

198 The data presented here are given in the standard delta notation, in per mil, reported relative to
199 JMC 3-0749 (Maréchal et al., 1999): $\delta^{66}\text{Zn} (\text{‰}) = [({}^{66}\text{Zn}/{}^{64}\text{Zn})_{\text{sample}} / ({}^{66}\text{Zn}/{}^{64}\text{Zn})_{\text{JMC-Lyon}}] - 1$.
200 Accuracy and precision were monitored relative to a secondary standard, IRMM-3702,
201 previously reported to yield a value of +0.32 ‰ (Cloquet et al., 2008; Ponzevera et al., 2006).
202 Relative to JMC-Lyon, we obtain $\delta^{66}\text{Zn} = 0.30 \pm 0.06 \text{ ‰}$ (2 SD, n = 163 over 380 days). All
203 our culturing results are reported as the fractionation observed between the medium and the
204 separated biomass, here denoted $\Delta^{66}\text{Zn} (\text{‰}) = \delta^{66}\text{Zn}_{\text{biomass}} - \delta^{66}\text{Zn}_{\text{medium}}$. Culture experiments

1
2
3
4
5
6
7
8
9
10
11
12
13
14
15
16
17
18
19
20
21
22
23
24
25
26
27
28
29
30
31
32
33
34
35
36
37
38
39
40
41
42
43
44
45
46
47
48
49
50
51
52
53
54
55
56
57
58
59
60
61
62
63
64
65

205 were only considered relevant for reporting when nearly 100% of the Zn initially added to the
206 medium was recovered in the residual medium plus the biomass fraction after the experiment,
207 as quantified by isotope dilution. All diagrams plot the external precision, based on replicate
208 analyses of IRMM-3702 as noted above, unless internal errors exceed the external
209 reproducibility.

210 **3. Results**

211 Based on measured growth and metal uptake data, the largest cultured diatom, *T. weissfloggi*,
212 reached Zn uptake rates up to about 26% of the maximum that could be supplied to the cell by
213 diffusion (Table 1). The prokaryotic organisms cultured here were much less likely to be
214 diffusion limited - and consistently contained less than 1% of the amount of Zn that could be
215 supplied by diffusion. Fe exerts a key control on phytoplankton growth and thus metal uptake
216 (Köbberich and Vance, 2017; Sunda and Huntsman, 1995; Sunda and Huntsman, 1997), so that
217 Table 1 also provides data supporting the suggestion that growth is not suppressed as a
218 consequence of diffusion limited Fe supply.

219 Three different diatom strains, each grown on nitrate and urea as the sole N source, were
220 generally found to grow fast, with specific growth rates between 0.65 and 0.77 d⁻¹. At identical
221 irradiance and nutrient levels, three representatives of the genus *Synechococcus* grew at more
222 variable rates, ranging from 0.42 to 0.82 d⁻¹ (Fig. 2A). *Prochlorococcus marinus* – the smallest
223 strain cultured here – grew at a specific growth rate of 0.28 d⁻¹, at half the irradiance level (25
224 μmol m⁻² s⁻¹) applied to all other strains (50 μmol m⁻² s⁻¹).

225 Fe uptake into marine phytoplankton has previously been shown to be a surface area related
226 process (Sunda and Huntsman, 1995; Sunda and Huntsman, 1997). Surface area normalized Fe
227 and Zn uptake rates, calculated from measured cellular quotas and the surface areas shown in
228 Fig. 1, are high and variable for diatoms, reaching up to values that are often greater than 100
229 nmol m⁻² d⁻¹. Those of prokaryotes are mostly much lower (Fig. 2B and C).

1
2
3
4
5
6
7
8
9
10
11
12
13
14
15
16
17
18
19
20
21
22
23
24
25
26
270 Carbon or P-normalized cellular Fe and Zn of all measured diatoms are in good agreement with
231 previous culture work (Sunda and Huntsman, 1992; Sunda and Huntsman, 1995) at similar
232 bioavailable metal concentrations. Measured metal to P quotas were converted to Zn/C
233 assuming a Redfield stoichiometry of C:P of 106:1. In good agreement with previous work on a
234 coastal *Synechococcus bacillaris* strain (Sunda and Huntsman, 2015), all studied cyanobacteria
235 yielded higher cellular Fe quotas than the majority of cultured diatoms (Fig. 3A), while their
236 absolute rates of metal transport across the cell membrane were generally found to be very low
237 (Fig. 2B). Except for the *Synechococcus* strain CCMP 2370, the opposite was found for cellular
238 Zn quotas (Fig. 3B), also at comparatively low uptake rates (Fig. 2C). This becomes most
239 apparent if cellular Zn quotas are plotted as a function of Fe quotas (Fig. 3C). Excluding CCMP
240 2370, the highest Zn/P quotas of $\sim 2 \text{ mmol mol}^{-1}$ were found with low Fe/P ratios, while the
241 lowest of $\sim 0.5 \text{ mmol mol}^{-1}$ were reached at Fe/P $\sim 7 \text{ mmol mol}^{-1}$.

242 All the isotope results are given in Table 1. The biomass of the marine diatom *T. oceanica*
243 shows a preference for light isotopes by 0.28‰, similar that previously observed for this strain
244 for a comparable culture medium ($\Delta^{66}\text{Zn}$; John et al., 2007; Köbberich and Vance, 2017).

245 **4. Discussion**

246 Of the two groups of organisms cultured here for Zn isotopes, the data for cyanobacteria are the
247 most novel. Previous studies have presented data for diatoms (John et al., 2007; Köbberich and
248 Vance, 2017; Köbberich and Vance, 2018), while Samanta et al. (2017) have published Zn
249 isotope data for another eukaryote group, the coccoliths. Thus, we first discuss the variation
250 within the cyanobacteria strains cultured, before moving on to compare these new data with the
251 new and published data for eukaryotes.

252 **4.1 Variations in metal uptake characteristics among cyanobacteria**

253 Three of the four cyanobacteria cultured were found to have similar cellular Zn quotas to
254 diatoms, though at the lower end of the latter's range. The opposite is true for cellular Fe quotas
255 (Fig. 3A and 3B), a finding which is in agreement with previous work (Saito et al., 2003; Sunda

1
2
3
4
5
6
7
8
9
10
11
12
13
14
15
16
17
18
19
20
21
22
23
24
25
26
27
28
29
30
31
32
33
34
35
36
37
38
256 and Huntsman, 2015; Sunda and Huntsman, 1995). It is also obvious from Fig. 3, that CCMP
257 2370 differs from the other cyanobacteria in its Zn quota. Though this difference is less marked
258 for Fe, it is also the case that the Fe quotas found for CCMP 2370 represent the higher end of
259 the observed spectrum (Fig. 3C). High biomass associated Fe contents might indicate the
260 presence of surface-bound Fe-hydroxides, which could adsorb large quantities of Zn, and this
261 theory might be supported by positive biomass $\Delta^{66}\text{Zn}$ values (see Table 1 and Section 4.3;
262 Gélabert et al., 2006; John et al., 2007). However, the variability in the overall cyanobacterial
263 dataset, for both Fe- and Zn-quotas and including the data for CCMP 2370, is no greater than
264 that seen in natural communities using X-ray fluorescence imaging techniques (Twining and
265 Baines, 2013). Moreover, Tang and Morel (2006) did not detect any increase in cellular Zn/P at
266 the total medium Fe concentrations used here, or for the biomass Fe/P ratios measured here. It
267 is also the case that CCMP 2370 differs from all other cyanobacteria in the greater proportion
268 of phycoerythrin (PE) in its total budget of chromophores (Six et al., 2007). There is,
269 however, currently no known Zn containing enzyme involved in the biosynthesis of PE.
270 Whether the cellular Zn content could be related to such biochemical pathways remains to be
271 addressed in future research (for additional thoughts see section S.5 of the Supplementary
272 Information).

39 273 **4.2 Similarities and differences between prokaryotic and eukaryotic metal uptake**

40
41
42
43
44
45
46
47
48
49
50
51
52
53
54
55
56
274 Culture experiments are performed in a controlled environment. An assessment of taxonomic
275 differences from such experiments is often only possible in terms of whether the phytoplankton
276 of interest is well adapted to the culture conditions used, coupled to a comparison between
277 those culturing conditions and the organism's natural habitat. Thus, despite an extensive body
278 of literature on the physiological response to various types of environmental stress (for a review
279 see Morel et al., 2014) applied in laboratory cultures, it remains challenging to separate purely
280 taxonomic effects from imposed environmental factors.

57
58
59
60
61
62
63
64
65
281 The precise culture conditions chosen here for the eukaryotic organisms were adjusted to yield
282 similar specific growth rates for each organism, using published constraints (Sunda and

1
2
3
4
5
6
7
8
9
10
11
12
13
14
15
16
17
18
19
20
21
22
23
24
25
26
27
28
29
30
31
32
33
34
35
36
37
38
39
40
41
42
43
44
45
46
47
48
49
50
51
52
53
54
55
56
57
58
59
60
61
62
63
64
65

283 Huntsman, 1995; Sunda and Huntsman, 1997). Thus, though the open ocean diatom *T.*
284 *oceanica*, as well as a representative of the genus *Chaetoceros*, grew at similar rates for the
285 same Fe', the same growth rates were only achieved for the coastal species, *T. weissflogii*, at Fe'
286 that was almost twice as high (Table 1). Prokaryotes such as the tiny *Prochlorococcus* simply
287 behave too differently to reasonably expect them to yield the same fast growth rates as diatoms
288 in culture (*c.f.* Supplementary Information S.1). In our experiments, CCMP 1183 and 2370
289 were at least close, though somewhat more variable (Fig. 2A).

290 **4.3 Ligand control on $\Delta^{66}\text{Zn}$ recorded in phytoplankton**

291 Based on precautions to avoid diffusion-limited Zn transport towards the cell surface (*c.f.*
292 section S.2 in the Supplementary Information), we can essentially exclude the possibility that
293 any of the negative $\Delta^{66}\text{Zn}$ observed here are likely to be caused by the slightly faster diffusion
294 rates of the lighter ^{64}Zn isotope. Only the cyanobacteria strain CCMP 2370, with unusually high
295 cellular Zn quotas, was found to yield positive $\Delta^{66}\text{Zn}$ values with respect to the bulk culture
296 medium (Fig. 4). All other phytoplankton, whether pro- or eukaryotic, consistently yielded
297 negative $\Delta^{66}\text{Zn}$ values (Table 1). These findings are in good agreement with previous culture
298 experiments (John et al., 2007; Köbberich and Vance, 2017; Samanta et al., 2017), at similar
299 bioavailable Zn levels, as illustrated in Fig. 5.

300 The equilibrium fractionation between Zn-EDTA and 'free' Zn is such that heavy Zn isotopes
301 are preferentially bound to the organic chelator (Ban et al., 2002; Ding et al., 2010a; Ding et al.,
302 2010b; Markovic et al., 2017), while the bioavailable Zn^{2+} pool is enriched in light Zn isotopes
303 - before any interaction with phytoplankton. In agreement with the suggestion of John et al.
304 (2007), we thus argue that a substantial portion of the observed $\Delta^{66}\text{Zn}$ in cultured
305 phytoplankton is actually the result of this equilibrium fractionation in the medium, rather than
306 resulting from biological uptake. Although there is strain-dependent variability in the extent to
307 which the light Zn isotope is taken up into phytoplankton, there are no systematic differences
308 between cyanobacteria and diatoms. In fact, excluding CCMP 2370, the absolute ranges
309 observed among different representatives of both clades are almost indistinguishable from each

1
2
3
4
5
6
7
8
9
10
11
12
13
14
15
16
17
18
19
20
21
22
23
24
25
26
27
28
29
30
31
32
33
34
35
36
37
38
39
40
41
42
43
44
45
46
47
48
49
50
51
52
53
54
55
56
57
58
59
60
61
62
63
64
65

310 other. Neither absolute rates of Zn transport across the cell surface area, nor A/V ratios (see
311 Supplementary Information, Fig. S.1), seem to correlate with the extent to which light Zn
312 isotopes are preferentially taken up. This could simply be due to the fact that the studied
313 diversity is still too small, obscuring any potential pattern. On the other hand, the uptake
314 mechanism may be important, given that there is an increasing preference for light Zn isotopes
315 as a result of additional active transport across the cell wall beyond the level associated with
316 high-affinity transporters alone (John et al., 2007). Thus, the observed variability might be
317 caused by the fact that the onset of low-affinity Zn uptake may occur at different bioavailable
318 Zn concentrations, as previously identified for *T. oceanica* (John et al., 2007) and *Emiliania*
319 *huxleyi* (Samanta et al., 2017). In this study, bioavailable Zn was chosen to be at the higher end
320 of the range previously considered relevant for high-affinity uptake (for a more detailed
321 discussion, see Köbberich and Vance, 2017). Thus, it is possible that light signatures seen in
322 some of the strains studied here might be explained by isotope fractionation associated with
323 active low-affinity transporters superimposed on a fractionation caused by the high-affinity
324 mechanism.

325 **5. Conclusion and oceanic implications**

326 The two first order features of the oceanic distributions of Zn isotopes that are emerging as data
327 accumulates are: 1) in the Southern Ocean, despite often dramatic drawdown of Zn at the
328 surface, mostly by diatoms, variations in the small residual Zn pool are very muted (*e.g.*, Wang
329 et al., this volume; Zhao et al., 2014); 2) outside the Southern Ocean, residual seawater tends to
330 be lighter in the upper ocean, seeming to imply the uptake of heavy isotopes (*e.g.*, Conway and
331 John, 2014), though where high depth resolution is available near the surface it is often the case
332 that these light values actually occur in the immediate sub-surface (*e.g.*, Wang et al., this
333 volume). Though variations in dissolved Zn isotopes in the surface Southern Ocean are indeed
334 muted, there is also a slight minimum at 100-200m (Wang et al., this volume). The above
335 observations are both, at first glance, inconsistent with the finding of light Zn isotopes in

1
2
3
4
5
6
7
8
9
10
11
12
13
14
15
16
17
18
19
20
21
22
23
24
25
26
27
28
29
30
31
32
33
34
35
36
37
38
39
40
41
42
43
44
45
46
47
48
49
50
51
52
53
54
55
56
57
58
59
60
61
62
63
64
65

336 phytoplankton cells in culture. Here we discuss each of the above observations of the real ocean
337 in turn, in the context of the summary of culturing experiments in Fig. 5.

338 An important conclusion from Fig. 5 is that a large proportion of the enrichment of light Zn in a
339 variety of studied pro- and eukaryotic phytoplankton can be explained by the presence of
340 organic ligands in culture media. Consistent with a postulate by John et al. (2007), heavy Zn
341 isotopes are preferentially bound to the trace metal buffer EDTA in culture media, while the
342 ‘free’ bioavailable Zn pool is already enriched in light isotopes before uptake. A significant
343 proportion of light Zn found in phytoplankton after a culture experiment might thus be the
344 result of an aqueous equilibrium in seawater, rather than the consequence of kinetic isotope
345 fractionation during active transport across the cell wall. Although the uncertainty on the
346 isotope fractionation associated with the relevant Zn-EDTA equilibrium is still large (Ban et al.,
347 2002; Ding et al., 2010a; Ding et al., 2010b; Markovic et al., 2017), kinetic isotope effects
348 associated with uptake are only rarely outside the range that could be explained by the presence
349 of this strong ligand.

350 One could argue that, since the real ocean also contains strong ligands that bind Zn, it is still the
351 $\Delta^{66}\text{Zn}$ fractionation with respect to bulk medium that is the most relevant for the great majority
352 of oceanic regimes. For example, Ellwood and Van den Berg (2000) have shown that 94 - 99%
353 of all Zn in the open NE Atlantic is bound to strong organic complexes. Free Zn concentrations
354 - at 6 - 20 pmol l^{-1} - in those regions are low, but not low enough to limit the growth of a typical
355 oceanic species (Ellwood and Van den Berg, 2000). Thus, the situation regarding complexation
356 of Zn in the real ocean is *qualitatively* analogous to that in culture experiments, with the
357 bioavailable pool being lighter than the ligand bound fraction.

358 In the surface Southern Ocean, Zn is rapidly drawn down by diatom uptake, by almost 2 orders
359 of magnitude relative to the upwelled deep waters (*e.g.*, Vance et al., 2017; Zhao et al., 2014).
360 If such uptake prefers the light isotope to the extent seen for $\Delta^{66}\text{Zn}_{\text{biomass} - \text{bulk medium}}$ in culturing
361 experiments (Fig. 5), then the $\delta^{66}\text{Zn}$ of the residual Zn-depleted water should exceed 1‰, when
362 in fact it barely rises above the deep ocean average $\delta^{66}\text{Zn}$ of +0.5‰ more than analytical

1
2
3
4
5
6
7
8
9
10
11
12
13
14
15
16
17
18
19
20
21
22
23
24
25
26
27
28
29
30
31
32
33
34
35
36
37
38
39
40
41
42
43
44
45
46
47
48
49
50
51
52
53
54
55
56
57
58
59
60
61
62
63
64
65

363 uncertainty (Wang et al., this volume; Zhao et al., 2014). It could be that the answer to this
364 problem originates with differences in the speciation of Zn in culture versus seawater.
365 Markovic et al. (2017) present experimental findings showing that isotope fractionation
366 between free Zn and the organically-bound complex depends on the thermodynamic stability
367 constant for that complex, which for EDTA is about 6 orders of magnitude greater than those
368 for Zn in the real ocean (*e.g.*, Bruland, 1989; Ellwood and van den Berg, 2000; Markovic et al.,
369 2017). However, Bruland (1989) also showed that the *conditional* stability constant for Zn-
370 EDTA complexes in seawater are lower than those for natural organic ligands, due to side
371 reactions between EDTA and Ca and Mg ions that do not occur for the natural ligands (Bruland
372 et al., 1989).

373 Finally, we turn to the apparently light Zn isotope values in areas outside the Southern Ocean.
374 John and Conway (2014) have suggested an explanation in terms of preferential loss of heavy
375 isotope through scavenging to particulate organic matter. One issue with this suggestion is that
376 the experiment in which scavenging, and Zn isotope fractionation associated with it, was
377 observed (John and Conway, 2014) contained none of the organic ligands that stabilize Zn in
378 solution, whereas most of the surface ocean contains more than 10 times more Zn-specific
379 ligands than total dissolved Zn found in the NE Atlantic (Ellwood and Van den Berg, 2000).
380 The one part of the surface ocean where this is known not to be the case is the Southern Ocean,
381 (Baars and Croot, 2011), and this is where heavy surface isotopes are not seen.

382 As shown in the data compilation in Wang et al. (this volume), most profiles with generally
383 negative $\delta^{66}\text{Zn}$ in the upper ocean actually feature a heavy value right at the surface. In at least
384 some cases, this upward move to heavy Zn isotopes is defined by more than a single sample.
385 We suggest, therefore, that the data are often consistent with uptake of slightly light isotopes at
386 the surface and that the light isotopes that apparently dominate the upper ocean in *e.g.* the
387 North Atlantic (Conway and John, 2014) are at least partially the result of very shallow sub-
388 surface (peaking at about 100 m but extending down to 500 m) regeneration of biomass-
389 associated light Zn isotopes (*e.g.*, Bermin et al., 2006). It is also clear, however, that mass

1
2
3
4
5
6
7
8
9
10
11
12
13
14
15
16
17
18
19
20
21
22
23
24
25
26
390 balance considerations mean that such a process cannot explain the overall light upper layer
391 outside the Southern Ocean - *i.e.* the upper 500m. This Southern Ocean biogeochemical divide
392 is emerging as a key feature of the ocean biogeochemistry of Zn, consistent with the behavior
393 of other nutrients in the ocean (*e.g.*, Marinov et al., 2006; Sarmiento et al., 2004; Vance et al.,
394 2017). The Zn-rich deep cycle is fed by deep waters that only re-connect to the surface in the
395 Southern Ocean, and sits below a rather isolated extra-Southern shallow ocean exhibiting
396 different processes. Recent studies have highlighted a very similar pattern for Cd and its
397 isotopes, with Cd isotopes apparently buffered to a surprisingly constant value in this low-
398 latitude surface pool (*e.g.*, Xie et al., 2017; Sieber et al., this volume). It is speculation at
399 present, but the idea that one of the processes that have been invoked for Cd, supply from the
400 atmosphere (Xie et al., 2017), could also explain light Zn in the low latitude surface merits
401 further investigation.

402 **Acknowledgements**

403 We are grateful to Alysia D. Cox for help with setting up a phytoplankton culturing lab at ETH
404 Zurich and to Timothy I. Eglinton for allowing us access to biology laboratories and incubator
405 facilities. We also wish to thank Corey Archer for valuable support with elemental and isotopic
406 analysis and Amélie Ritscher for her work as a research assistant at ETH Zurich. Financial
407 support was provided by ETH and the Swiss National Science Foundation (SNF) through grant
408 200021-143262.

409 **References**

- 410 Archer, C., Vance, D., 2004. Mass discrimination correction in multiple-collector plasma
411 source mass spectrometry: an example using Cu and Zn isotopes. *Journal of Analytical*
412 *Atomic Spectrometry*, 19: 656-665.
- 413
414 Baars, O., Croot, P.L., 2011. The speciation of dissolved zinc in the Atlantic sector of the
415 Southern Ocean. *Deep Sea Research Part II: Topical Studies in Oceanography*, 58:
416 2720-2732.
- 417
418 Ban, Y., Aida, M., Nomura, M., Fujii, Y., 2002. Zinc isotope separation by ligand exchange
419 chromatography using cation exchange resin. *Journal of Ion Exchange*, 13: 46-52.

420

1 421 Bermin, J., Vance, D., Archer, C., Statham, P.J., 2006. The determination of the isotopic
2 422 composition of Cu and Zn in seawater. *Chemical Geology*, 226: 280-297.

3 423

4 424 Brand, L.E., 1991. Minimum iron requirements of marine phytoplankton and the implications
5 425 for the biogeochemical control of new production. *Limnology and Oceanography*, 36:
6 426 1756-1771.

7 427

8 428 Bruland, K.W., 1980. Oceanographic distributions of cadmium, zinc, nickel, and copper in the
9 429 North Pacific Earth and Planetary Science Letters, 47: 176-198.

10 430

11 431 Bruland, K.W. (1989) Complexation of zinc by natural organic ligands in the central North
12 432 Pacific. *Limnology and Oceanography* 34: 269-285.

13 433

14 434 Bruland, K.W., Middag, R., Lohan, M.C., 2014. Controls of trace metals in seawater. In:
15 435 Heinrich, D.H., Karl, K.T. (Eds.), *Treatise on Geochemistry*. Elsevier, Oxford, pp. 19-
16 436 51.

17 437

18 438 Buitenhuis, E.T. et al., 2013. MAREDAT: towards a world atlas of MARine Ecosystem DATA.
19 439 *Earth System Science Data*, 5: 227-239.

20 440

21 441 Cloquet, C., Carignan, J., Lehmann, M., Vanhaecke, F., 2008. Variation in the isotopic
22 442 composition of zinc in the natural environment and the use of zinc isotopes in
23 443 biogeosciences: a review. *Analytical and Bioanalytical Chemistry*, 390: 451-463.

24 444

25 445 Conway, T.M., John, S.G., 2014. The biogeochemical cycling of zinc and zinc isotopes in the
26 446 North Atlantic Ocean. *Global Biogeochemical Cycles*, 28: 1111-1128.

27 447

28 448 Conway, T.M., John, S.G., 2015. The cycling of iron, zinc and cadmium in the North East
29 449 Pacific Ocean – insights from stable isotopes. *Geochimica et Cosmochimica Acta*, 164:
30 450 262-283.

31 451

32 452 Cox, A.D., Saito, M.A., 2013. Proteomic responses of oceanic *Synechococcus* WH8102 to
33 453 phosphate and zinc scarcity and cadmium additions. *Frontiers in Microbiology*, 4: 387,
34 454 pp. 1-17.

35 455

36 456 Ding, X., Nomura, M., Fujii, Y., 2010a. Zinc isotope effects by chromatographic chelating
37 457 exchange resin. *Progress in Nuclear Energy*, 52: 164-167.

38 458

39 459 Ding, X., Nomura, M., Suzuki, T., Fujii, Y., 2010b. Chromatographic zinc isotope separation
40 460 by chelating exchange resin. *Chromatographia*, 71: 195-199.

41 461

42 462 Domsic, J.F. et al., 2008. Entrapment of Carbon Dioxide in the Active Site of Carbonic
43 463 Anhydrase II. *Journal of Biological Chemistry*, 283: 30766-30771.

44 464

45 465 Ellwood, M.J., Van den Berg, C.M.G., 2000. Zinc speciation in the Northeastern Atlantic
46 466 Ocean. *Marine Chemistry*, 68: 295-306.

47

48

49

50

51

52

467

468 Falkowski, P.G., Knoll, A.H., 2007. Evolution of primary producers in the sea. Elsevier
469 Academic Press.

470

471 Follows, M.J., Dutkiewicz, S., Grant, S., Chisholm, S.W., 2007. Emergent Biogeography of
472 Microbial Communities in a Model Ocean. *Science*, 315: 1843-1846.

473

474 Follows, M.J., Dutkiewicz, S., 2010. Modeling Diverse Communities of Marine Microbes.
475 *Annual Review of Marine Science*, 3: 427-451.

476

477 Gélabert, A. et al., 2006. Interaction between zinc and freshwater and marine diatom species:
478 surface complexation and Zn isotope fractionation. *Geochimica et Cosmochimica Acta*,
479 70: 839-857.

480

481 Hopkinson, B.M., Barbeau, K.A., 2008. Interactive influences of iron and light limitation on
482 phytoplankton at subsurface chlorophyll maxima in the eastern North Pacific.
483 *Limnology and Oceanography*, 53: 1303-1318.

484

485 John, S.G., Geis, R.W., Saito, M.A., Boyle, E.A., 2007. Zinc isotope fractionation during high-
486 affinity and low-affinity zinc transport by the marine diatom *Thalassiosira oceanica*.
487 *Limnology and Oceanography*, 52: 2710-2714.

488

489 John, S.G., Conway, T.M., 2014. A role for scavenging in the marine biogeochemical cycling
490 of zinc and zinc isotopes. *Earth and Planetary Science Letters*, 394: 159-167.

491

492 John, S.G., Helgoe, J., Townsend, E., 2018. Biogeochemical cycling of Zn and Cd and their
493 stable isotopes in the Eastern Tropical South Pacific. *Marine Chemistry* 201: 256-262.

494

495 Knoll, A.H., Canfield, D.E., Konhauser, K.O. (Eds.), 2012. *Fundamentals of Geobiology*. John
496 Wiley & Sons, Ltd., pp. 443.

497

498 Köbberich, M., Vance, D., 2017. Kinetic control on Zn isotope signatures recorded in marine
499 diatoms. *Geochimica et Cosmochimica Acta*, 210: 97-113.

500

501 Köbberich, M., Vance, D., 2018. Zinc association with surface-bound iron-hydroxides on
502 cultured marine diatoms: A zinc stable isotope perspective. *Marine Chemistry*.

503

504 Leblanc, K. et al., 2012. A global diatom database – abundance, biovolume and biomass in the
505 world ocean. *Earth System Science Data*, 4: 149-165.

506

507 Little, S.H., Vance, D., McManus, J., Severmann, S., 2016. Key role of continental margin
508 sediments in the oceanic mass balance of Zn and Zn isotopes. *Geology*, 44: 207-210.

509

510 Maréchal, C.N., Télouk, P., Albarède, F., 1999. Precise analysis of copper and zinc isotopic
511 compositions by plasma-source mass spectrometry. *Chemical Geology*, 156: 251-273.

512

1
2
3
4
5
6
7
8
9
10
11
12
13
14
15
16
17
18
19
20
21
22
23
24
25
26
27
28
29
30
31
32
33
34
35
36
37
38
39
40
41
42
43
44
45
46
47
48
49
50
51
52
53
54
55
56
57
58
59
60
61
62
63
64
65

- 1 513 Marinov, I., Gnanadesikan, A., Toggweiler, J.R., Sarmiento, J.L., 2006. The Southern Ocean
2 514 biogeochemical divide. *Nature*, 441: 964-967.
- 3 515
4 516 Markovic, T. et al., 2017. Experimental determination of zinc isotope fractionation in
5 517 complexes with the phytosiderophore 2'-deoxymugeneic acid (DMA) and its structural
6 518 analogues, and implications for plant uptake mechanisms. *Environmental Science &*
7 519 *Technology*, 51: 98–107.
- 8 520
9 521 Menemenlis, D. et al., 2005. NASA supercomputer improves prospects for ocean climate
10 522 research. *Eos, Transactions American Geophysical Union*, 86: 89-96.
- 11 523
12 524 Moore, C.M. et al., 2013. Processes and patterns of oceanic nutrient limitation. *Nature*
13 525 *Geoscience*, 6: 701-710.
- 14 526
15 527 Morel, F.M.M., 2008. The co-evolution of phytoplankton and trace element cycles in the
16 528 oceans. *Geobiology*, 6: 318-324.
- 17 529
18 530 Morel, F.M.M., Milligan, A.J., Saito, M.A., 2014. Marine bioinorganic chemistry: the role of
19 531 trace metals in the oceanic cycles of major nutrients. In: Heinrich, D.H., Karl, K.T.
20 532 (Eds.), *Treatise on Geochemistry*. Elsevier, Oxford, pp. 123-150.
- 21 533
22 534 O'Brien, C.J. et al., 2013. Global marine plankton functional type biomass distributions:
23 535 coccolithophores. *Earth System Science Data*, 5: 259-276.
- 24 536
25 537 Österberg, R., 1974. Origins of metal ions in biology. *Nature*, 249: 382-383.
- 26 538
27 539 Ponzevera, E. et al., 2006. Mass discrimination during MC-ICPMS isotopic ratio
28 540 measurements: investigation by means of synthetic isotopic mixtures (IRMM-007
29 541 series) and application to the calibration of natural-like zinc materials (Including
30 542 IRMM-3702 and IRMM-651). *Journal of the American Society for Mass Spectrometry*,
31 543 17: 1413-1428.
- 32 544
33 545 Roberts, S.B., Lane, T.W., Morel, F.M.M., 1997. Carbonic anhydrase in the marine diatom
34 546 *Thalassiosira weissflogii* (Bacillariophyceae). *Journal of Phycology*, 33: 845-850.
- 35 547
36 548 Saito, M.A., Sigman, D.M., Morel, F.M.M., 2003. The bioinorganic chemistry of the ancient
37 549 ocean: the co-evolution of cyanobacterial metal requirements and biogeochemical
38 550 cycles at the Archean–Proterozoic boundary? *Inorganica Chimica Acta*, 356: 308-318.
- 39 551
40 552 Samanta, M., Ellwood, M.J., Sinoir M., Hassler C.S., 2017. Dissolved zinc isotope cycling in
41 553 the Tasman Sea, SW Pacific Ocean. *Marine Chemistry*: 192: 1-12.
- 42 554
43 555 Samanta, M., Ellwood, M.J., Strzepek, R.F., 2017. Zinc isotope fractionation by *Emiliania*
44 556 *huxleyi* cultured across a range of free zinc ion concentrations. *Limnology and*
45 557 *Oceanography*: 63: 660-671.
- 46 558
47
48
49
50
51
52
53
54
55
56
57
58
59
60
61
62
63
64
65

- 1 559 Sarmiento, J.L., Gruber, N., Brzezinski, M.A., Dunne, J.P., 2004. High-latitude controls of
2 560 thermocline nutrients and low latitude biological productivity. *Nature*, 427: 56-60.
3 561
- 4 562 Sedwick, P.N., Church, T.M., Bowie, A.R., Marsay, C.M., Ussher, S.J., Achilles, K.M.,
5 563 Lethaby, P.J., Johnson, R.J., Sarin, M.M., McGillicuddy, D.J. (2005), Iron in the
6 564 Sargasso Sea (Bermuda Atlantic Time-series Study region) during summer: Eolian
7 565 imprint, spatiotemporal variability, and ecological implications, *Global*
8 566 *Biogeochemical Cycles*, 19, GB4006.
9 567
- 10 568 Shaked, Y., Xu, Y., Leblanc, K., Morel, F.M.M., 2006. Zinc availability and alkaline
11 569 phosphatase activity in *Emiliana huxleyi*: Implications for Zn-P co-limitation in the
12 570 ocean. *Limnology and Oceanography*, 51: 299-309.
13 571
- 14 572 Sieber, M., Conway, T.M., de Souza, G.F., Obata, H., Takano, S., Sohrin, Y., Vance, D., in
15 573 press. Physical and biogeochemical controls on the distribution of dissolved cadmium
16 574 and its isotopes in the Southwest Pacific Ocean. *Chemical Geology*, this volume.
17 575
- 18 576 Siebert, C., Nägler, T.F., Kramers, J.D., 2001. Determination of molybdenum isotope
19 577 fractionation by double-spike multicollector inductively coupled plasma mass
20 578 spectrometry. *Geochemistry, Geophysics, Geosystems*, 2: 1032.
21 579
- 22 580 Six, C. et al., 2007. Diversity and evolution of phycobilisomes in marine *Synechococcus spp.*: a
23 581 comparative genomics study. *Genome Biology*, 8: R259 pp. 1-22.
24 582
- 25 583 Smayda, T.J., 1978. From phytoplankters to biomass. In: Sournia, A. (Ed.), *Phytoplankton*
26 584 *manual*. Museum National d'Histoire Naturelle, Paris, pp. 273-279.
27 585
- 28 586 Sun, J., Liu, D., 2003. Geometric models for calculating cell biovolume and surface area for
29 587 phytoplankton. *Journal of Plankton Research*, 25: 1331-1346.
30 588
- 31 589 Sunda, W.G., Huntsman, S.A., 1992. Feedback interactions between zinc and phytoplankton in
32 590 seawater. *Limnology and Oceanography*, 37: 25-40.
33 591
- 34 592 Sunda, W.G., Huntsman, S.A., 1995. Iron uptake and growth limitation in oceanic and coastal
35 593 phytoplankton. *Marine Chemistry*, 50: 189-206.
36 594
- 37 595 Sunda, W.G., Huntsman, S.A., 1997. Interrelated influence of iron, light and cell size on marine
38 596 phytoplankton growth. *Nature*, 390: 389-392.
39 597
- 40 598 Sunda, W.G., Price, N.M., Morel, F.M.M., 2005. Trace metal ion buffers and their use in
41 599 culture studies. In: Andersen, R.A. (Ed.), *Algal Culturing Techniques*. Academic Press,
42 600 Burlington.
43 601
- 44 602 Sunda, W., Huntsman, S., 2015. High iron requirement for growth, photosynthesis, and low-
45 603 light acclimation in the coastal cyanobacterium *Synechococcus bacillaris*. *Frontiers in*
46 604 *Microbiology*, 6: 561.
47 605

1
2
3
4
5
6
7
8
9
10
11
12
13
14
15
16
17
18
19
20
21
22
23
24
25
26
27
28
29
30
31
32
33
34
35
36
37
38
39
40
41
42
43
44
45
46
47
48
49
50
51
52
53
54
55
56
57
58
59
60
61
62
63
64
65

606 Tang, D., Morel, F.M.M., 2006. Distinguishing between cellular and Fe-oxide-associated trace
607 elements in phytoplankton. *Marine Chemistry*, 98: 18-30.

608

609 Twining, B.S. et al., 2003. Quantifying trace elements in individual aquatic protist cells with a
610 synchrotron X-ray fluorescence microprobe. *Analytical Chemistry*, 75: 3806-3816.

611

612 Twining, B.S., Baines, S.B., 2013. The trace metal composition of marine phytoplankton.
613 *Annual Review of Marine Science*, 5: 191-215.

614

615 Vance, D. et al., 2016a. The oceanic budgets of nickel and zinc isotopes: the importance of
616 sulfidic environments as illustrated by the Black Sea. *Philosophical Transactions of the*
617 *Royal Society A: Mathematical, Physical and Engineering Sciences*, 374: 1-26.

618

619 Vance, D. et al., 2016b. The behaviour of Cu and Zn isotopes during soil development: controls
620 on the dissolved load of rivers. *Chemical Geology*, 445: 36-53.

621

622 Vance, D. et al., 2017. Silicon and zinc biogeochemical cycles coupled through the Southern
623 Ocean. *Nature Geoscience*, 10: 202-206.

624

625 Wang, R.M., Archer, C., Bowie, A.R., Vance, D., in press. Zinc and nickel isotopes in seawater
626 from the Indian Sector of the Southern Ocean: the impact of natural iron fertilization
627 versus Southern Ocean hydrography and biogeochemistry. *Chemical Geology*, this
628 volume.

629

630 Wolfe-Simon, F., Grzebyk, D., Schofield, O., Falkowski, P.G., 2005. The role and evolution of
631 superoxide dismutases in algae. *Journal of Phycology*, 41: 453-465.

632

633 Xie, R.C., Galer, S.J.G., Abouchami, W., Rijkenberg, M.J.A., de Baar, H.J.W., De Jong, J.,
634 Andreae, M.O., 2017. Non-Rayleigh control of upper-ocean Cd isotope fractionation in
635 the western South Atlantic, *Earth and Planetary Science Letters*, 471: 94-103.

636

637 Zhao, Y., 2011. The carbon cycle and bioactive trace metals in the oceans: constraints from
638 zinc isotopes. Dissertation, University of Bristol.

639

640 Zhao, Y., Vance, D., Abouchami, W., de Baar, H.J.W., 2014. Biogeochemical cycling of zinc
641 and its isotopes in the Southern Ocean. *Geochimica et Cosmochimica Acta*, 125: 653-
642 672.

643

644 **Figure captions**

1
2
3 645 *full page: Table 1.* Measured Fe and Zn uptake rates, cellular quotas, use efficiencies, and Zn
4
5 646 isotope results ($\Delta^{66}\text{Zn}_{\text{biomass} - \text{medium}} = \delta^{66}\text{Zn}_{\text{biomass}} - \delta^{66}\text{Zn}_{\text{medium}}$).

6
7
8 647 *two-column fitting image: Fig. 1.* Comparison of surface area to biovolume (A/V) ratios for all
9
10 648 phytoplankton cultured here to the ranges observed in natural communities as derived from
11
12 649 MARine Ecosystem DATa (MAREDAT; Buitenhuis et al., 2013).

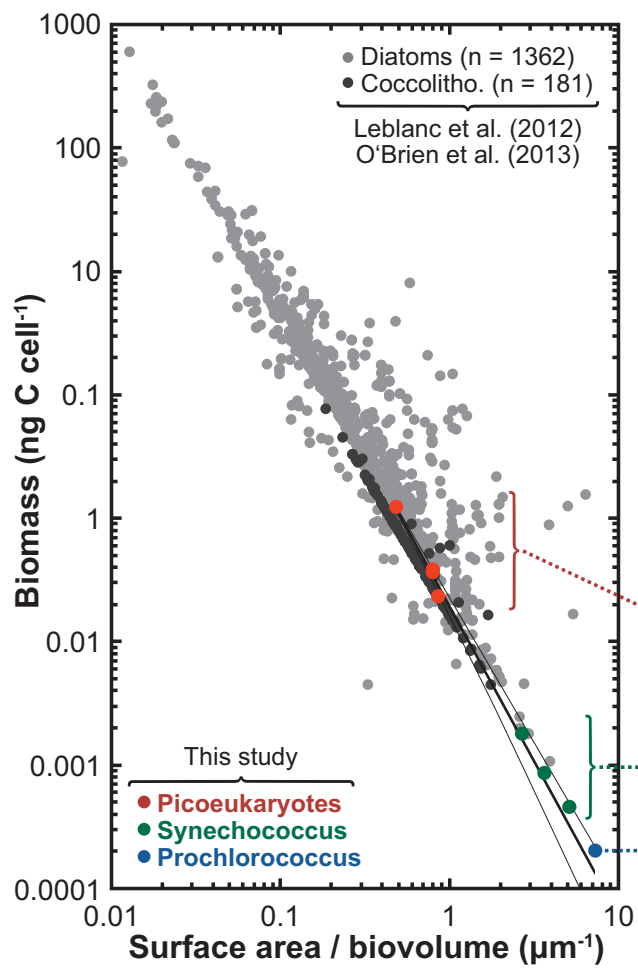
13
14
15 650 *single-column fitting image: Fig. 2.* Specific growth and metal uptake rates as a function of
16
17 651 A/V ratios for all cultured diatoms and cyanobacteria.

18
19
20 652 *single-column fitting image: Fig. 3.* Cellular Fe and Zn quotas as a function of A/V ratios (A
21
22 653 and B) and their interdependency (C) for all cultured diatoms and cyanobacteria.

23
24
25 654 *single-column fitting image: Fig. 4.* $\Delta^{66}\text{Zn}$ fractionation of cyanobacteria, which are variably
26
27 655 well adapted to the applied nutrient and light conditions as a result of their different light
28
29 656 harvesting strategies.

30
31
32 657 *two-column fitting image: Fig. 5.* Comparison of the Zn isotope fractionation upon uptake for
33
34 658 all phytoplankton studied here, along with data from the literature. The red band indicates the
35
36 659 range of $\Delta^{66}\text{Zn}$ values that could be explained simply by the presence of EDTA as a strong
37
38 660 organic chelator in the culture medium, and published data for Zn isotope separation between
39
40 661 Zn-EDTA and Zn^{2+} (Ban et al., 2002; Ding et al., 2010a; Ding et al., 2010b; Markovic et al.,
41
42 662 2017).
43
44
45
46
47
48
49
50
51
52
53
54
55
56
57
58
59
60
61
62
63
64
65

Figure 1



Picoeukaryotes

T. weissflogii (1336)

1616 μm³, 778 μm²
A / V: 0.48 μm⁻¹

Chaetoceros sp. (199)

346 μm³, 275 μm²
A / V: 0.79 μm⁻¹

T. oceanica (1005)

331 μm³, 265 μm²
A / V: 0.80 μm⁻¹

E. huxleyii (371)

179.6 μm³, 154 μm²
A / V: 0.86 μm⁻¹

Synecho ...

... coccus sp. (1183)

6.28 μm³, 16.9 μm²
A / V: 2.69 μm⁻¹

... coccus sp. (2370)

1.77 μm³, 7.07 μm²
A / V: 4.00 μm⁻¹

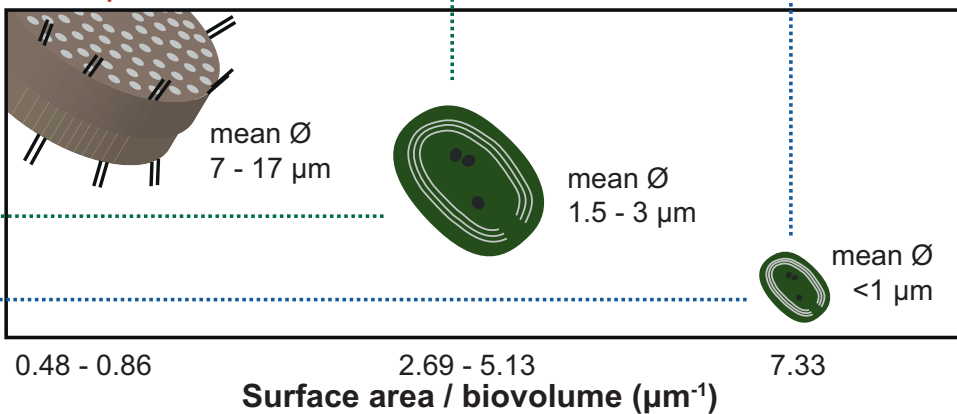
... coccus sp. (1334)

1.05 μm³, 5.37 μm²
A / V: 5.13 μm⁻¹

Prochloro ...

... coccus sp. (2389)

0.36 μm³, 2.63 μm²
A / V: 7.33 μm⁻¹



A Figure 2

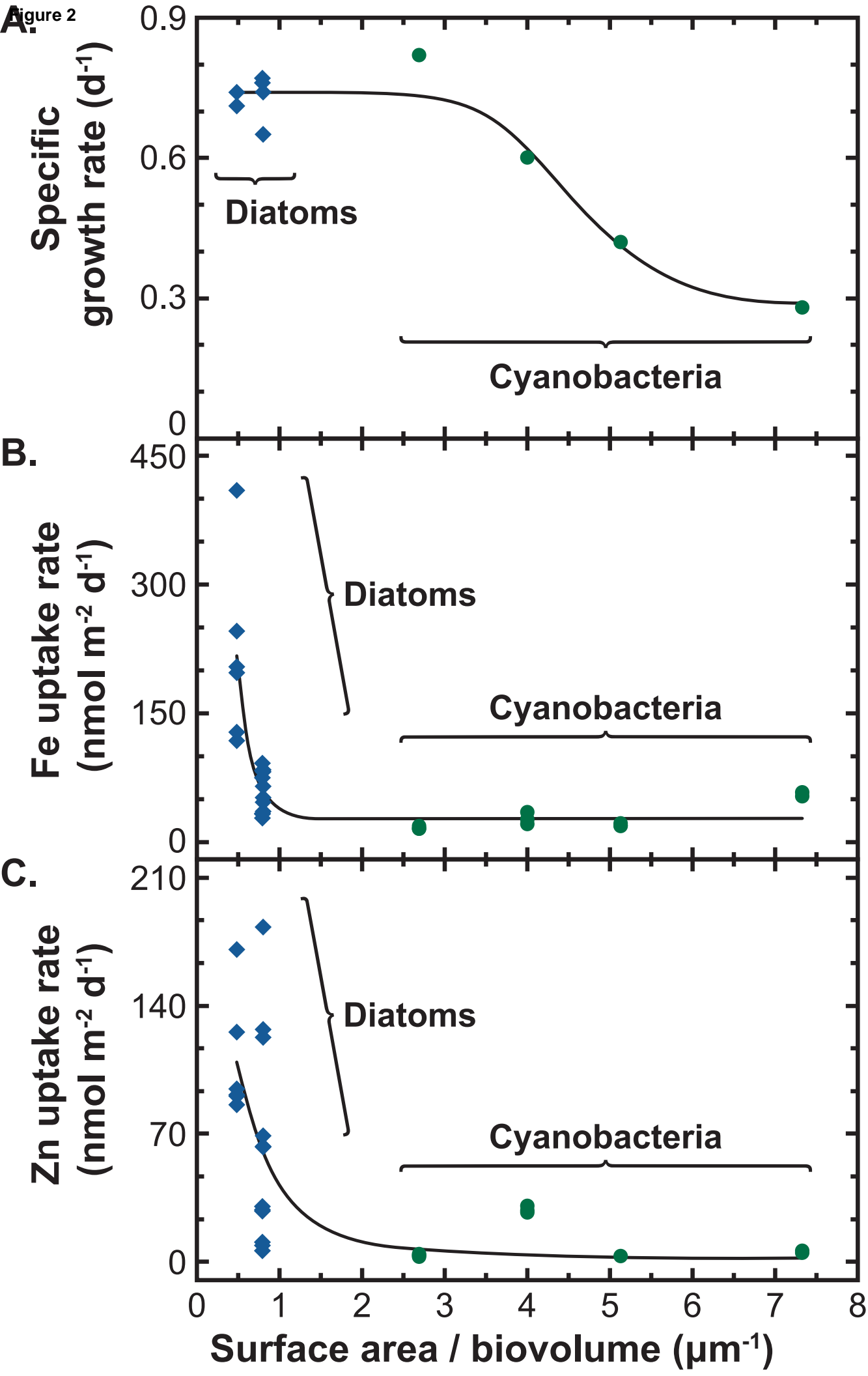


Figure 3 Diatoms Cyanobacteria

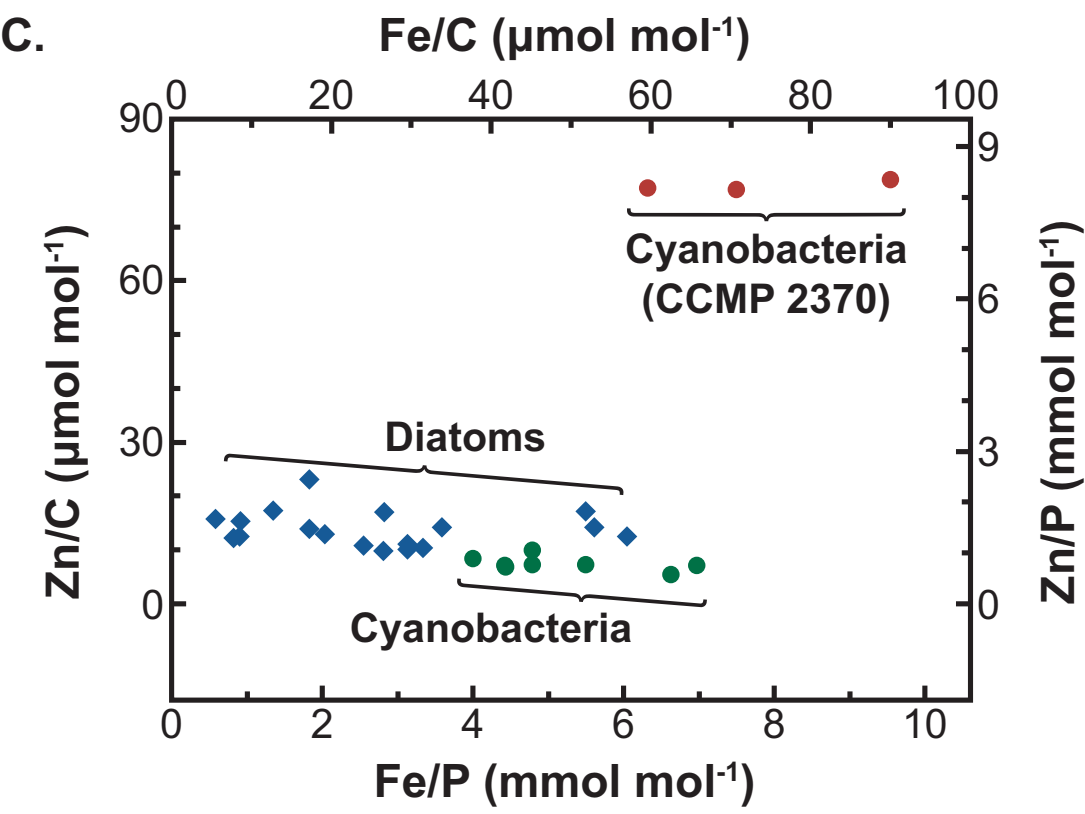
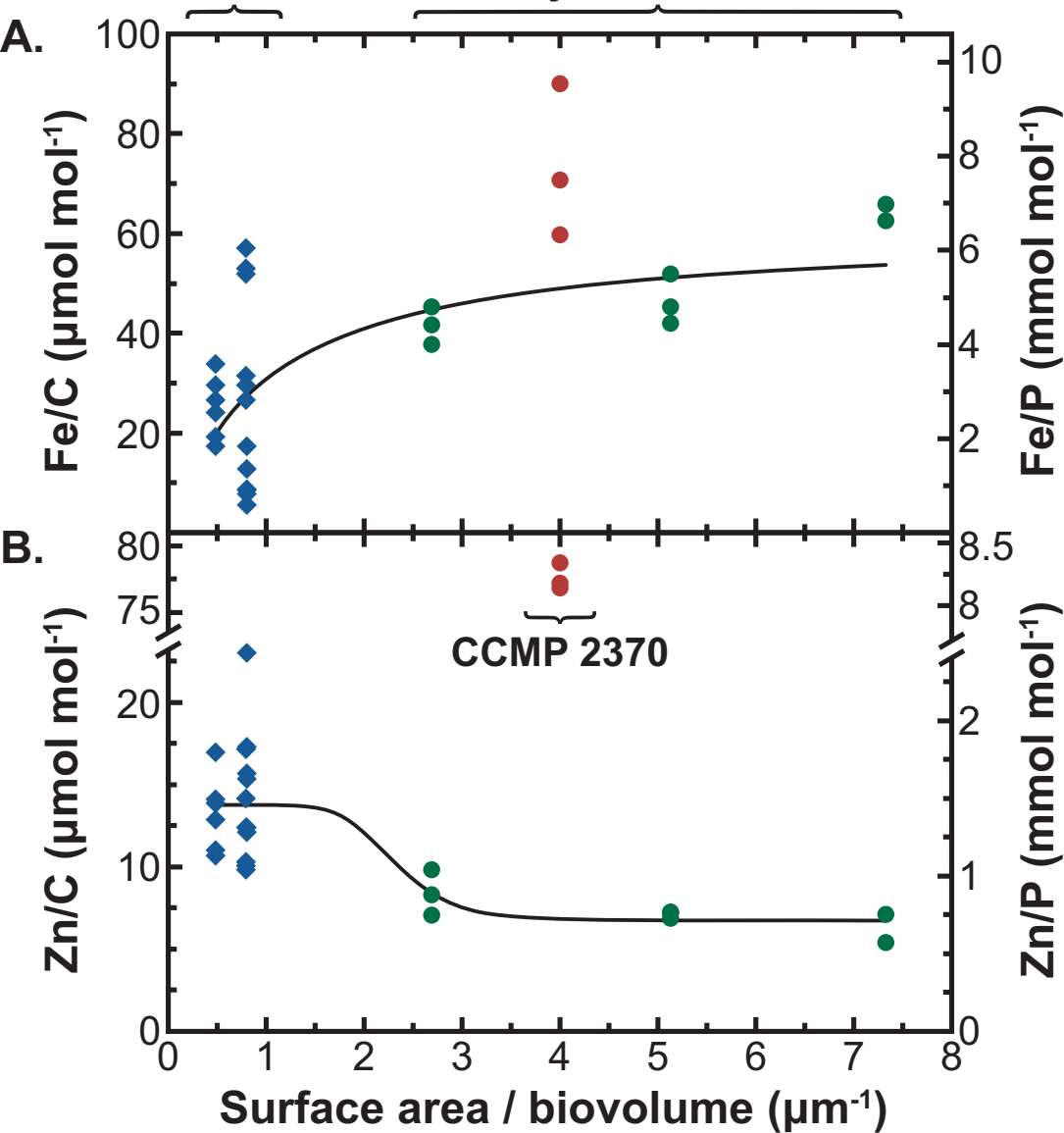


Figure 4

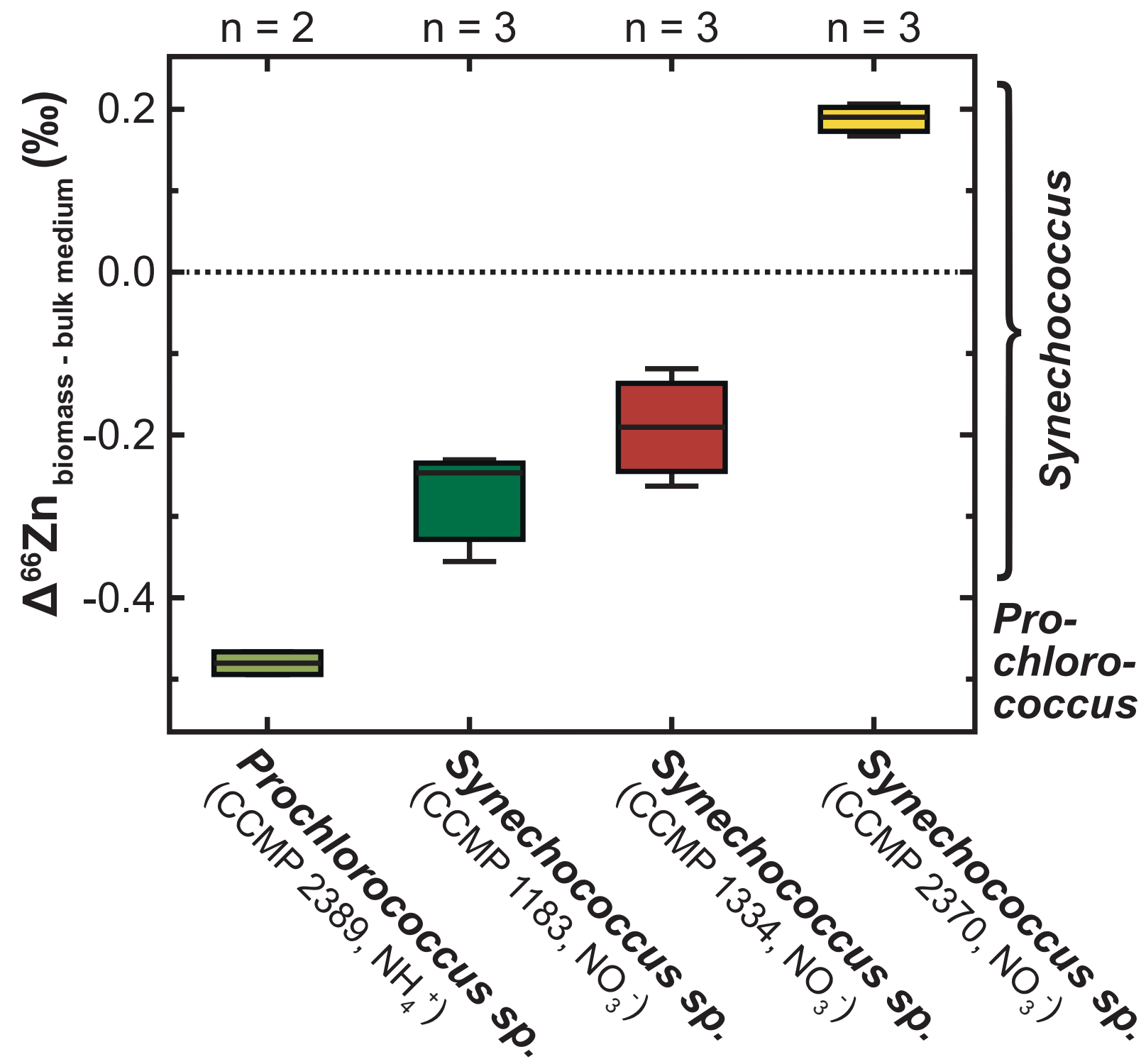


Figure 5

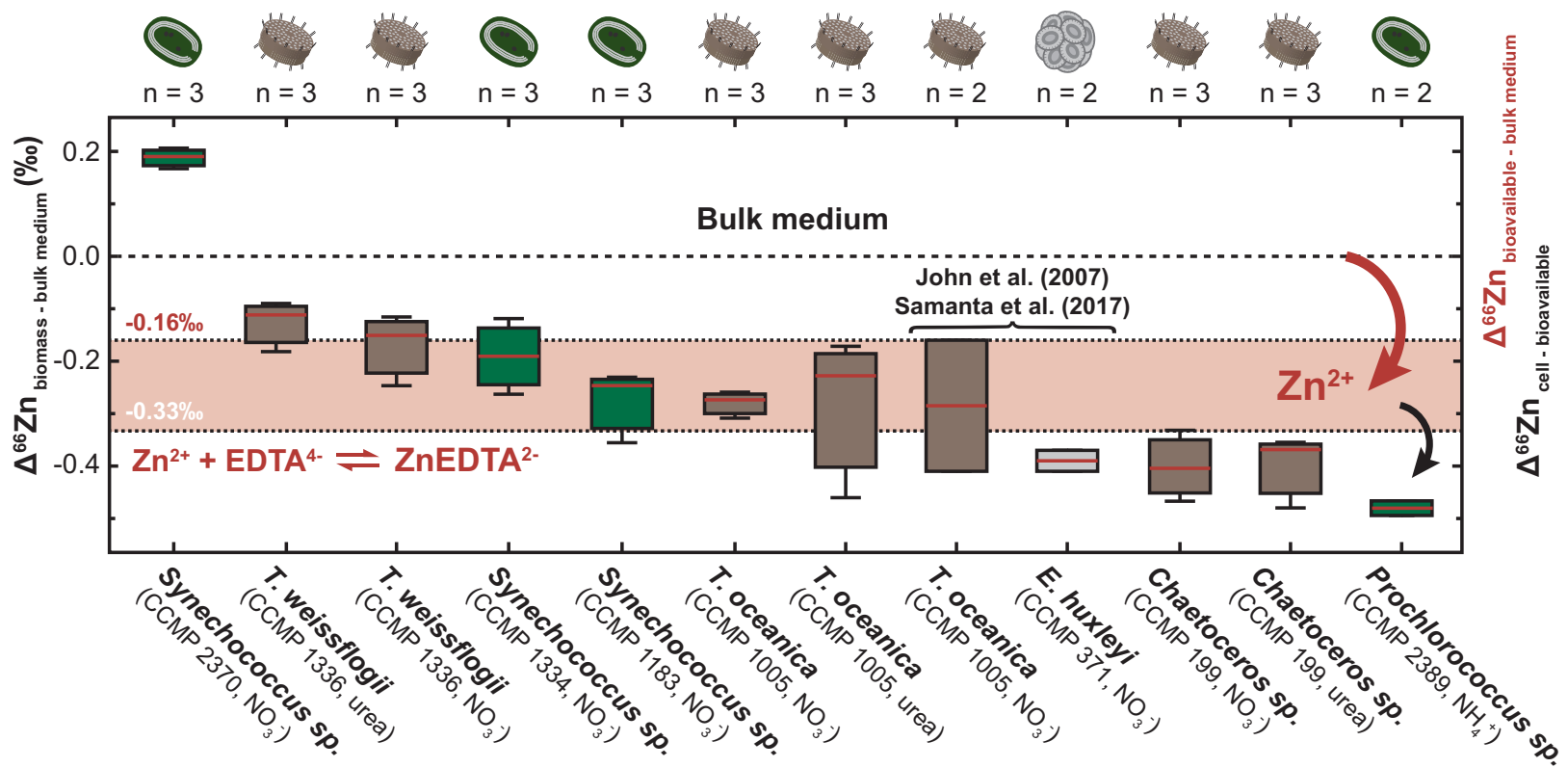


Figure S.1

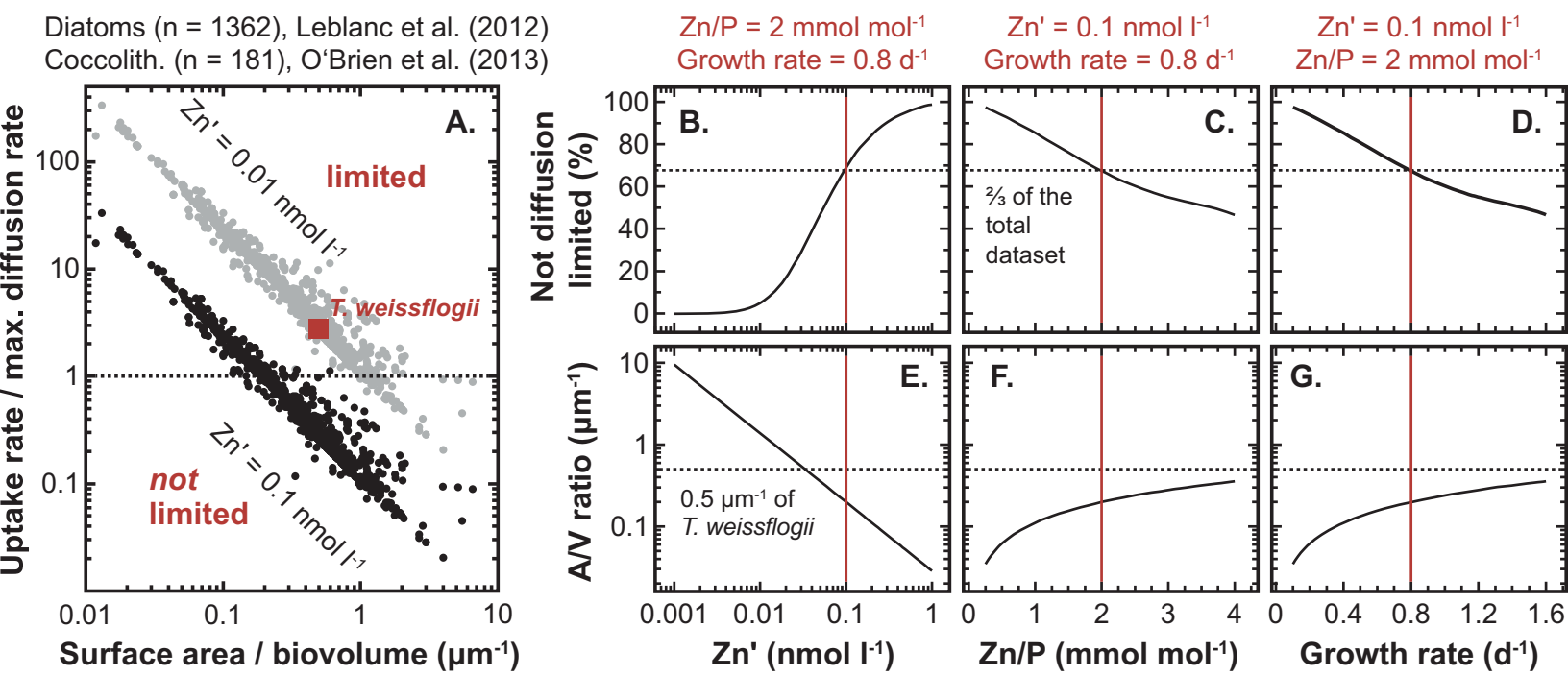


Figure S.2

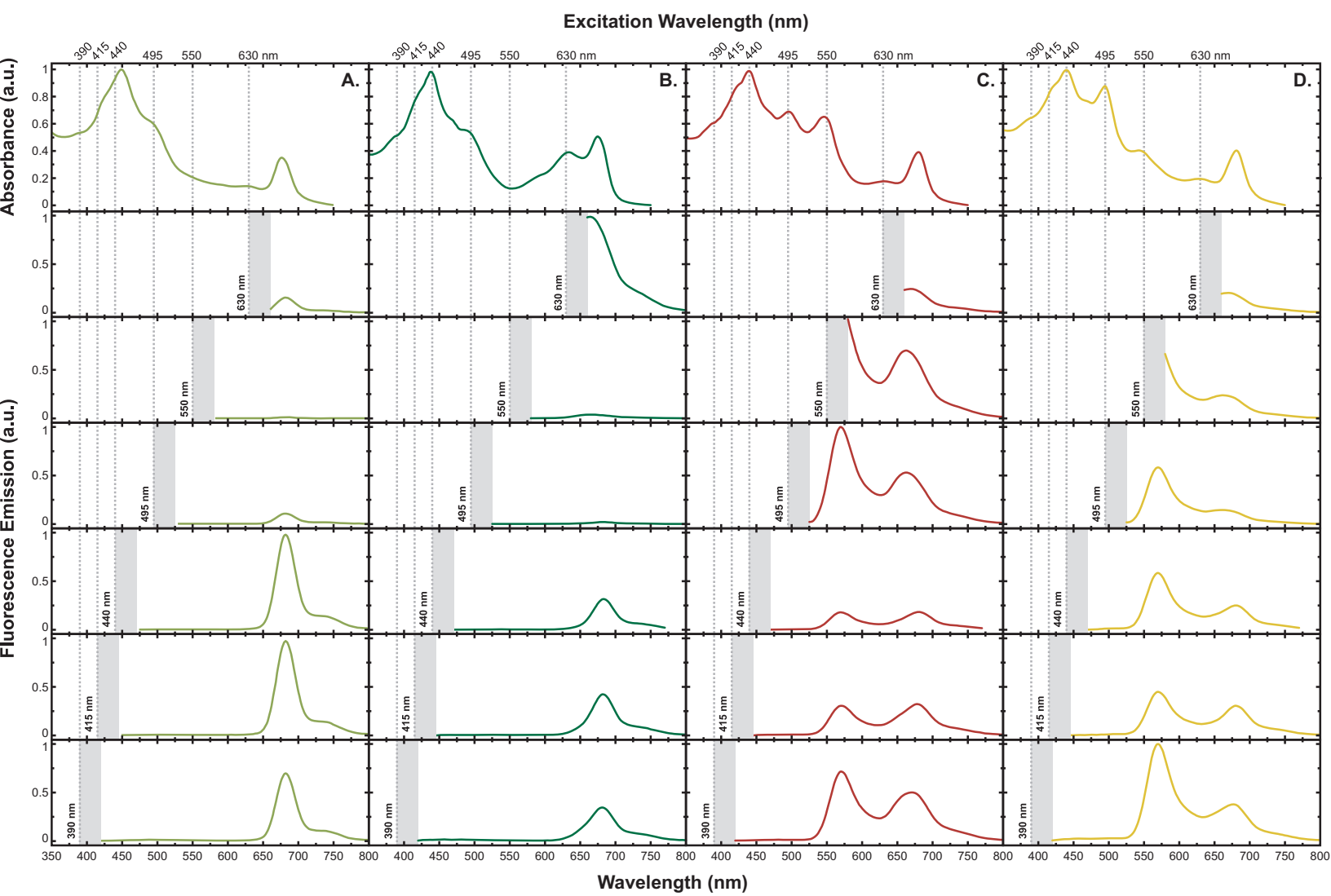


Figure S.3

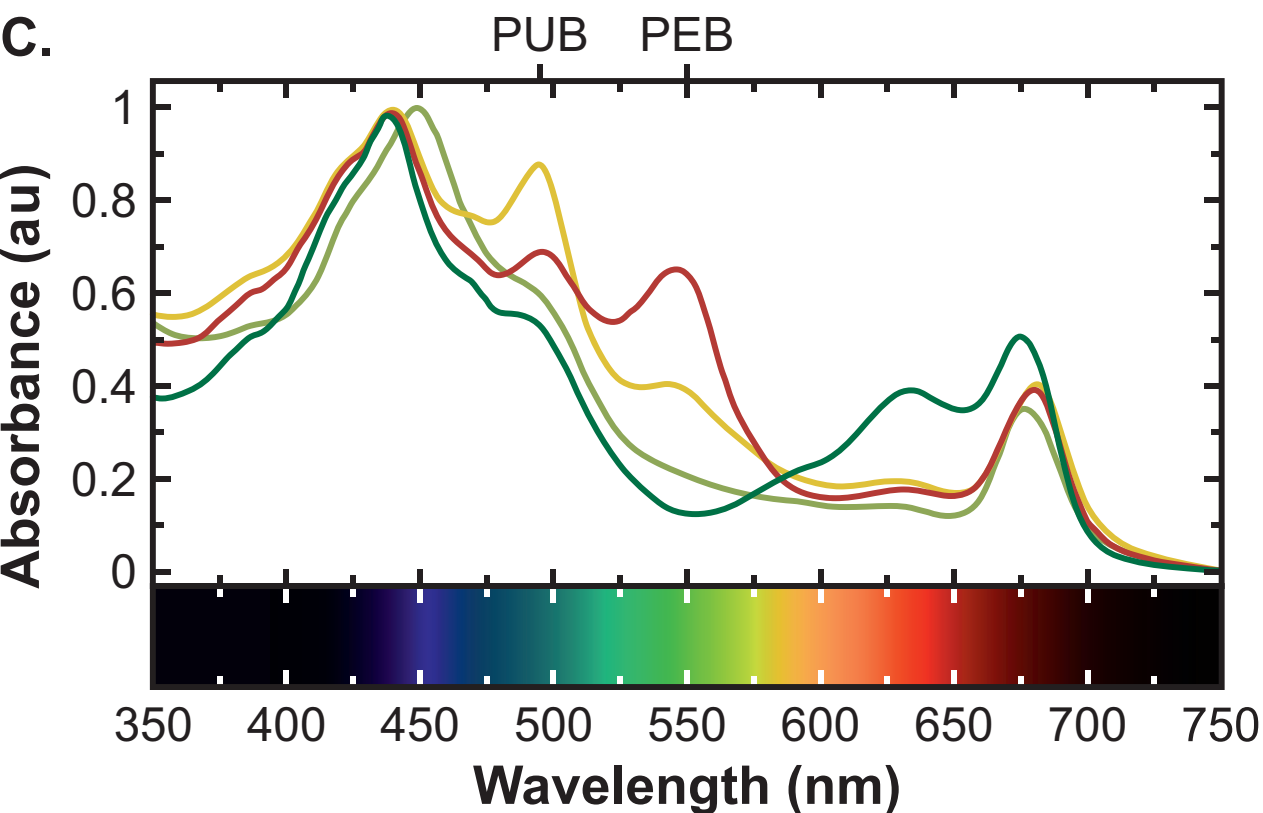
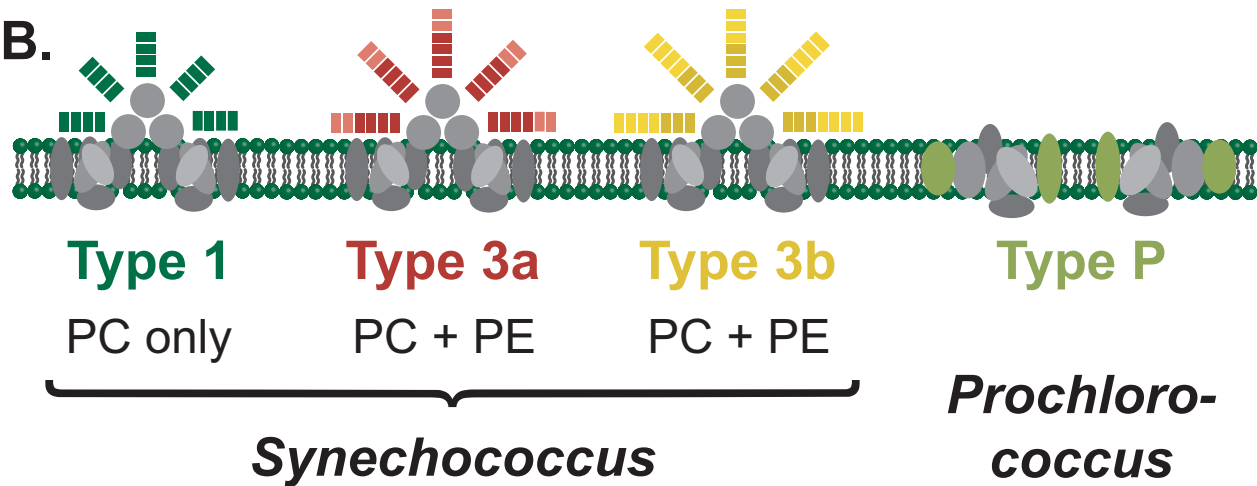


Figure S.4

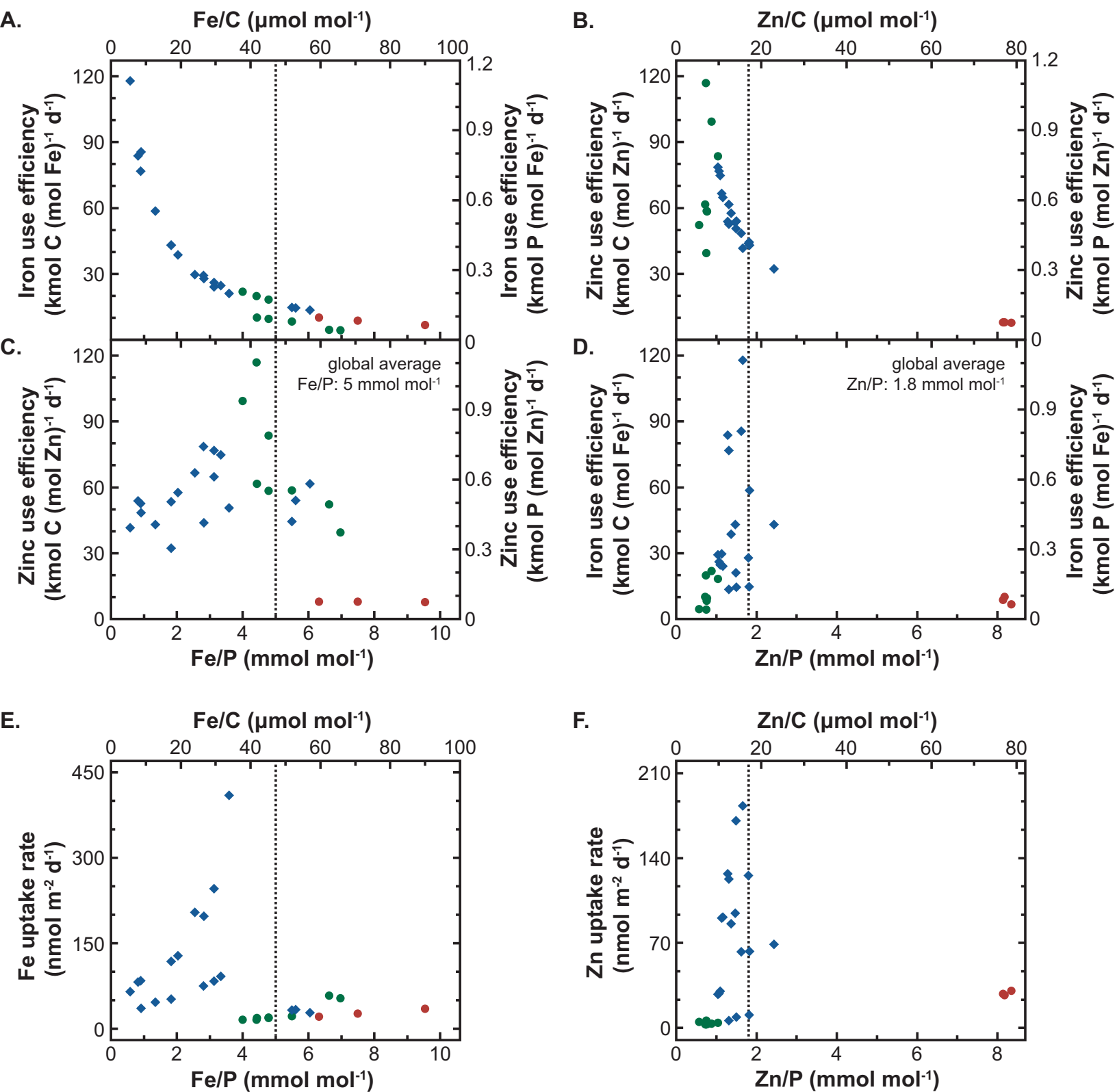


Table 1

[Click here to download Table: table 1.eps](#)

Species / Strain	A/V	Shape	Growth conditions				Uptake rates **		Cell. quota		Use efficiency †		Diffusion ‡		Zn isotopes	
			N source	Fe'	Zn'	μ^*	Fe	Zn	Fe/P	Zn/P	IUE	ZUE	Fe'	Zn'	$\Delta^{66}\text{Zn}$	2 σ
	μm^{-1}			pmol l ⁻¹ ...		d ⁻¹	nmol m ⁻² d ⁻¹ ...		mmol mol ⁻¹ ...		kmol P (mol M) ⁻¹ d ⁻¹ ...	%	%	‰	‰	
Diatoms	0.48	cylinder	nitrate	367	109	0.74	246	91.2	3.13	1.16	0.226	0.610	7.31	13.8	-0.25	0.09
							204	90.5	2.55	1.13	0.278	0.627	6.06	13.7	-0.15	0.09
							409	170	3.58	1.49	0.198	0.476	12.2	25.7	-0.12	0.07
			urea	378	106	0.71	117	94.3	1.83	1.47	0.404	0.503	3.40	14.6	-0.11	0.07
							128	85.6	2.03	1.36	0.364	0.543	3.69	13.2	-0.18	0.11
							197	125	2.82	1.79	0.263	0.412	5.70	19.4	-0.09	0.07
	0.79	cylinder	nitrate	190	102	0.77	74.2	27.5	2.81	1.04	0.274	0.741	2.53	2.62	-0.47	0.06
							91.8	30.1	3.34	1.09	0.231	0.705	3.13	2.86	-0.33	0.06
							83.2	28.3	3.13	1.06	0.246	0.724	2.84	2.69	-0.40	0.07
			urea	178	100	0.76	33.3	8.89	5.61	1.50	0.135	0.508	1.21	0.86	-0.35	0.16
							27.5	5.97	6.05	1.31	0.126	0.580	1.00	0.58	-0.37	0.18
							32.0	10.6	5.49	1.82	0.138	0.418	1.16	1.02	-0.48	0.17
0.80	cylinder	nitrate	190	102	0.74	35.3	62.5	0.92	1.62	0.807	0.455	1.18	5.82	-0.27	0.03	
						46.2	63.0	1.34	1.83	0.551	0.404	1.54	5.87	-0.26	0.04	
						51.6	68.9	1.83	2.44	0.405	0.304	1.72	6.42	-0.31	0.04	
		urea	178	100	0.65	81.5	127	0.82	1.28	0.790	0.507	2.90	12.0	-0.17	0.06	
						83.7	122	0.90	1.31	0.724	0.495	2.98	11.6	-0.23	0.05	
						64.5	183	0.59	1.66	1.111	0.392	2.30	17.3	-0.46	0.07	
Cyanobacteria	2.69	prolate spheroid	nitrate	173	102	0.82	15.6	2.63	4.42	0.74	0.186	1.101	0.14	0.06	-0.36	0.11
							18.3	3.99	4.79	1.04	0.171	0.787	0.16	0.09	-0.25	0.08
							15.3	3.37	3.99	0.88	0.205	0.936	0.13	0.08	-0.23	0.09
	4.00	sphere	nitrate	173	102	0.60	34.7	30.3	9.54	8.34	0.063	0.072	0.19	0.43	0.21	0.03
							25.8	28.0	7.49	8.14	0.080	0.074	0.14	0.40	0.17	0.04
							20.8	26.9	6.32	8.18	0.095	0.073	0.12	0.38	0.19	0.05
	5.13	prolate spheroid	nitrate	173	102	0.42	18.8	3.07	4.44	0.72	0.095	0.579	0.09	0.04	-0.26	0.07
							19.6	3.13	4.78	0.76	0.088	0.549	0.10	0.04	-0.19	0.07
							21.2	2.93	5.50	0.76	0.076	0.551	0.11	0.04	-0.12	0.09
	7.33	prolate spheroid	ammonia	1198	139	0.28	53.2	5.75	6.96	0.75	0.040	0.372	0.03	0.04	-0.49	0.04
							57.4	4.93	6.62	0.57	0.042	0.492	0.03	0.03	-0.47	0.04

* Including volumetric and handling errors we estimate the specific growth rate of replicates to have an uncertainty of less than ± 0.05 d⁻¹. ** Metal uptake rates are calculated after Sunda & Huntsman (1995, 1997), here normalized to the surface area of the cell. † Metal use efficiencies are computed by dividing the specific growth rate by the cellular metal to phosphorus ratio, analogous to Raven (1990) and Sunda & Huntsman (2015). Iron (IUE) and zinc use efficiencies (ZUE) refer to the molar quantities of phosphorus build up per mole of metal, given in kmol P (mol Fe)⁻¹ d⁻¹ and kmol P (mol Zn)⁻¹ d⁻¹, respectively. ‡ Diffusion limitation has been estimated by comparing cellular metal uptake rates with maximum diffusion rates, following recipes introduced by Hudson & Morel (1990) and Sunda & Huntsman (1992). The tabulated results are given as a percentage of the cellular uptake rate over the maximum diffusion rate, calculated with diffusion rate constants of $9 \cdot 10^{-6}$ cm² s⁻¹ (Hudson & Morel, 1990) and $6 \cdot 10^{-6}$ cm² s⁻¹ (Sunda & Huntsman, 1992), for Fe' and Zn', respectively. This calculation is further described in Section S.2.